

## Key Points:

- The sea level and current anomalies at both the western and eastern Indonesian Throughflow pathways correlate significantly with Niño 3.4
- Current anomalies in the two pathways respond oppositely to El Niño or La Niña signals
- Nonlinear processes modulate the relative importance of the two pathways in transmitting oceanic waves from the Pacific

## Supporting Information:

Supporting Information may be found in the online version of this article.

## Correspondence to:

H. Xue,  
hixue@xmu.edu.cn

## Citation:

Hu, X., Xue, H., & Liang, L. (2022). Impact of ENSO on the entrance of the Indonesian Throughflow: The oceanic wave propagation. *Journal of Geophysical Research: Oceans*, 127, e2022JC018782. <https://doi.org/10.1029/2022JC018782>

Received 23 APR 2022

Accepted 16 NOV 2022

## Author Contributions:

**Data curation:** Huijie Xue, Linlin Liang

**Formal analysis:** Xiaoyue Hu

**Funding acquisition:** Xiaoyue Hu, Huijie Xue

**Investigation:** Xiaoyue Hu, Huijie Xue

**Methodology:** Xiaoyue Hu, Huijie Xue

**Project Administration:** Huijie Xue

**Resources:** Huijie Xue, Linlin Liang

**Supervision:** Huijie Xue

**Writing – original draft:** Xiaoyue Hu

**Writing – review & editing:** Xiaoyue Hu, Huijie Xue

# Impact of ENSO on the Entrance of the Indonesian Throughflow: The Oceanic Wave Propagation

Xiaoyue Hu<sup>1</sup> , Huijie Xue<sup>2</sup> , and Linlin Liang<sup>3</sup>

<sup>1</sup>State Key Laboratory of Tropical Oceanography, South China Sea Institute of Oceanology, Chinese Academy of Sciences, Guangzhou, China, <sup>2</sup>State Key Lab of Marine Environmental Science, College of Ocean and Earth Sciences, Xiamen University, Xiamen, China, <sup>3</sup>Earth, Ocean and Atmospheric Sciences Thrust, The Hong Kong University of Science and Technology (Guangzhou), Guangzhou, China

**Abstract** A regional ocean model simulation for the period from 2000 through 2016 is used to study oceanic wave propagation in the Indonesian seas. The model simulation compares favorably with the interannual variability of the satellite derived sea level anomaly and the observed currents in the entrance passages of ITF. Lag correlation analysis suggests that the interannual sea level anomaly and opposite responses of the velocity above and below the thermocline in the western (the Sulawesi Sea and the Makassar Strait) and eastern (the Halmahera Sea) pathways of ITF are associated with the ENSO induced Rossby waves from the equatorial Pacific rather than the local wind forcing. In particular, during La Niña years ENSO induced anomalies traveling through the western pathway are comparable to those through the traditional eastern waveguide, suggesting the importance of both pathways in the propagation of ENSO signals in the Indonesian seas. Different roles of the western and eastern pathways in transmitting the ENSO signals into the Indonesian seas are associated with the nonlinear processes in the Sulawesi Sea, which appears to be linked with different states of the western boundary currents during the warm and cold ENSO phases.

**Plain Language Summary** Impacts of ENSO on the Indonesian seas that connect the Pacific and Indian Oceans at low latitudes, play an important role in interactions between the two oceans. Traditional understanding of the propagation of ENSO signals into the Indonesian seas is through the Halmahera Sea (i.e., the eastern pathway). In this work, we investigated the interannual sea level and current variations in the Indonesian seas using observations and a regional ocean model. We found both the eastern and western (via the Sulawesi Sea then the Makassar Strait) pathways have significant responses to ENSO signals via the propagating Rossby and Kelvin waves. More ENSO induced oceanic waves propagate through the western pathway during the La Niña years than the El Niño years concurrent with the penetrating state of the western boundary currents and weakened nonlinear processes in the Sulawesi Sea.

## 1. Introduction

Located between the tropical Indian and Pacific Oceans, the Indonesian seas provide the only oceanic connection for the two ocean basins at the low latitudes. The Indonesian Throughflow (ITF), driven by the pressure gradient between the two basins, transports surface and subsurface Pacific water into the Indian Ocean (Gordon, 2005). On the other hand, the recent works by Liang and Xue (2020) and J. Wang et al. (2020), which combined the in situ mooring observations at the exit straits (Sprintall et al., 1999, 2009) and in the Maluku Channel (Yuan et al., 2018), suggested a transport from the Indian Ocean to the Pacific Ocean at 500–2,000 m depths through the eastern Indonesian seas. These transports not only facilitate the heat, mass, and material exchanges between the Indian and Pacific Oceans, but also modulate the climate variability in warm-pool region and the whole planet (Godfrey, 1996; Gordon, 2005; Schneider, 1998; Sprintall et al., 2014; C. Wang, 2019; Yuan et al., 2011, 2013).

The Indonesian seas are one of the most significant oceanic pathways for the interactions between the interannual variability in the Pacific and Indian Oceans, such as the El Niño–Southern Oscillation (ENSO) signals and the Indian Ocean Dipole (IOD). In the ocean, IOD could have impact on the Pacific Ocean by the propagation of the Indian Ocean Kelvin waves through the Indonesian Seas (Yuan et al., 2013). Using observations and models, previous studies have proposed the general mechanisms for ENSO to affect the Indian Ocean: During the El Niño/La Niña events, easterly trade winds in the Pacific Ocean weaken/strengthen, which depress/raise the sea level in the western Pacific Ocean. As a result, the pressure gradient between the Indian and Pacific Oceans

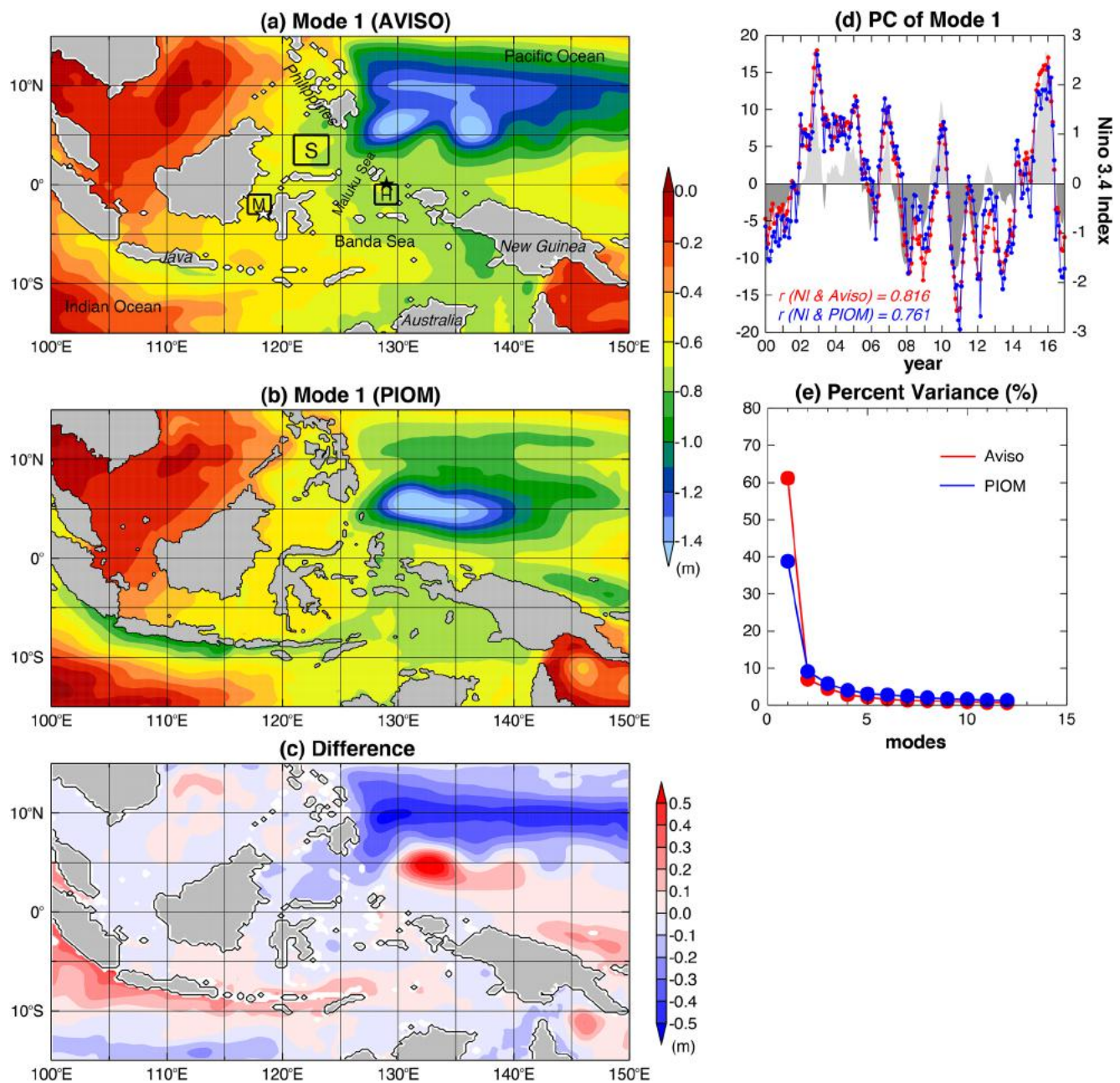


**Figure 1.** The empirical orthogonal function (EOF) pattern of the first mode of the interannual sea level anomalies (m) from AVISO altimetry product (a) and simulated by PIOM regional ocean model (b) during 2000–2016. Panel (c) is the difference between (a) and (b) (AVISO minus PIOM). Together with the principal components of the first EOF mode (d), and the percent variances of the first 12 modes (e). Black boxes in (a) indicate the sub-regions of the Makassar Strait (M), the Sulawesi Sea (S), and the Halmahera Sea (H) used in later figures. White and black stars in (a) mark the locations of the Makassar and Halmahera moorings, respectively. Gray shadows in (d) represent the Niño 3.4 index.

decreases/increases, inducing a corresponding decrease/increase in the ITF heat and mass transport into the Indian Ocean (Clarke & Liu, 1994; England & Huang, 2005; D. Hu et al., 2015; Liu et al., 2015; Meyers, 1996; Sprintall et al., 2014; Yuan et al., 2013). Owing to the Arlindo program (Gordon et al., 1998), the International Nusantara Stratification and Transport program (INSTANT, Sprintall et al., 2004), and Monitoring the ITF program (MITF, Gordon et al., 2019), the interannual variability of the ITF transport in the main western inflow passage, that is, the Makassar Strait (labeled in Figure 1a), was revealed, which confirmed the response of the ITF to ENSO (Gordon et al., 1999, 2008, 2012, 2019; M. Li et al., 2020; Susanto & Gordon, 2005; Susanto et al., 2012). Ultimately, in the oceanic channel, the ENSO signals propagating into the Indian Ocean

impact on the variability in the Indian Ocean such as the Madden-Julian Oscillation, the Indian Ocean Dipole (Saji et al., 1999), and the Ningaloo Niño/Niña via the Indonesian seas (Feng et al., 2013; Kataoka et al., 2014; Kusunoki et al., 2020; Zhang & Han, 2018), besides the atmospheric bridge (Alexander et al., 2002; Izumo et al., 2010; Klein et al., 1999; Lau & Nath, 2003).

As a part of the leaky Pacific Ocean western boundary, the Indonesian seas also represent a crossroad for planetary waves from the Pacific to the Indian Ocean, making it possible for the ENSO signals to travel to the Indian Ocean through wave propagation. ENSO-related wind anomalies generate equatorial Rossby waves that propagate westward to the western boundary of the Pacific Ocean and arrive at the Indonesian seas via linear (Clarke, 1991; du Penhoat & Cane, 1991) and nonlinear (Spall & Pedlosky, 2005; Yuan et al., 2004) dynamics. Based on these theories, about one third of the energy is reflected back as Kelvin waves to the Pacific Ocean, and the remainder continue to propagate as the coastal Kelvin waves along the Philippines into the Sulawesi Sea (X. Hu et al., 2019; M. Li, Xue, et al., 2021) (referred as the western waveguide in this study), or travel southward through the Halmahera Sea, then along the New Guinea—Australian shelf (labeled in Figure 1a) and finally into the southeast Indian Ocean (McClean et al., 2005; Wijffels & Meyers, 2004) (referred as the eastern waveguide in this study). The Maluku Sea (labeled in Figure 1a) may be another important connection of the Indo-Pacific Oceans in the eastern Indonesian seas at interannual time scales (X. Hu et al., 2019; X. Li, Yuan, et al., 2021; Yuan et al., 2022). Particularly, nonlinear dynamics of Rossby wave propagation at the leaky western boundary are determined by the leaping or penetrating state of the western boundary current (WBC) of the Pacific Ocean (Yuan et al., 2019). Based on a series of studies on the hysteresis of the eddies colliding with WBC at the entrance of the ITF (Z. Wang & Yuan, 2012, 2014; Yuan & Wang, 2011), Yuan et al. (2019) found that a leaping WBC blocks nearly all westward propagating eddies, whereas if the WBC is in a penetrating state, the Rossby waves may propagate uninterrupted through the gap. The recent study of X. Li, Yuan, et al. (2021) confirmed the nonlinear process using mooring observations in the Maluku Sea during 2016–2017.

Moreover, X. Li et al. (2020) reported that during 2016 and 2017 the seasonal transport in the Jailolo Strait (marked in Figure 1a as the black star) was much larger than the year-to-year differences and further concluded the interannual anomalies from the Pacific Ocean to the Indian Ocean might not pass through the Halmahera Sea, whereas M. Li, Xue, et al. (2021) reported a strong intrusion in the Makassar Strait in the sub-thermocline layer during 2016–2017. Limited by the length of the observations, X. Li et al. (2020) only put forward a challenge to the existing theory of the eastern waveguide during the observation period. Detailed dynamics of how ENSO anomalies propagate to the Indian Ocean through the Indonesian seas, and specific contributions of the eastern and the western waveguide during different ENSO phases still need to be investigated.

In this study, we focus on the propagation of the Pacific Ocean ENSO signals into the Indonesian seas using the satellite-derived sea surface height, a three-dimensional primitive equation regional ocean model, as well as a linear continuously stratified ocean model. Data products and models are introduced in Section 2. The interannual sea level and velocity variations at both passages are presented in Section 3. Based on the interannual anomalies, the propagation of the ENSO signal at the entrance of ITF during different ENSO phases are investigated in Section 4, followed by the discussions of the specific pathways in the Indonesian seas and interannual signals from the Indian Ocean in Section 5. Summary of this study is provided in Section 6.

## 2. Data and Models

### 2.1. Observed Data

To validate the model and investigate the interannual sea level variability in the Indonesian seas, we use the Archiving, Validation and Interpretation of Satellite Oceanographic (AVISO) altimeter sea level product in this study. The AVISO merged sea level anomaly (SLA) product used in this study is now managed by the Copernicus Marine and Environment Monitoring Service (CMEMS), from January 1993 to present, covering the global ocean with a horizontal resolution of  $1/4^\circ$ . We use the daily mean product released by AVISO, which is further averaged into monthly means when compared with the simulated data.

We use the blended sea winds developed by National Climatic Data Center (NCDC), National Oceanic and Atmospheric Administration (NOAA) in this study to extract the local wind variability, which is the same wind forcing that drives the 3D regional ocean model and the linear continuously stratified model. The blended sea



winds synthesize information from multiple satellites to improve the resolution and accuracy. The data set we use is 0.25° gridded data covering the global oceans, with daily resolution from July 1987 to October 2018.

The observed velocity data used in this study are from recent mooring observations in the Indonesian seas. We choose data collected from moorings deployed in the western and eastern routes of the ITF: in the Makassar Strait during INSTANT and MITF programs (Gordon et al., 2019) and in the Halmahera Sea during the IOCAS-RCO/LIPI joint cruise (X. Li et al., 2020). Hereafter we refer these two datasets as the Makassar data and the Halmahera data, respectively. The daily Makassar data are from moorings located in the Labani Channel around 3°S and 118.5°E (the white star in Figure 1a) from January 2004 to August 2017 with a data gap from August 2011 to August 2013, and are interpolated onto 20-m vertical grids from 40 to 760 m depths. The Halmahera data are 120-day low-pass filtered data from moorings deployed in the Jailolo Strait near 129°E on the equator (the black star in Figure 1a) from November 2015 to October 2017. The vertical profiles cover the depth range from 0 to 1,000 m with a 10-m interval. The Makassar data and the corresponding model velocity when compared with the mooring data are also filtered by using a 120-day low-pass filter, the same as the one applied to the Halmahera data.

## 2.2. The 3D Regional Ocean Model

The western Pacific and northern Indian Oceans Model (PIOM) is first reported by Liang et al. (2019). It has already been successfully used in studies of the circulation in the Banda Sea (Liang et al., 2019) and the Reversal Indian Ocean Waters (Liang & Xue, 2020). The model is based on the Regional Ocean Modeling System (ROMS), and it covers the region from 20°S to 52°N, 35° to 157°E, including the northern Indian Ocean, the western Pacific Ocean, and the entire Indonesian seas. The model has a horizontal resolution of 1/12°, and 30 levels in the vertical from a stretched and generalized terrain-following sigma coordinate. In this study, we use the real-time daily output between January 2000 and December 2016, from a simulation forced by the NCDC daily blended sea winds. More detailed information about the model is documented in Liang et al. (2019).

## 2.3. The Linear Continuously Stratified Model (LCSM)

The LCSM (McCreary, 1981) is also used to simulate the ocean circulation in the Indonesian seas to compare with the PIOM simulation. The LCSM is the same as the one used in Yuan and Han (2006), and it has been successfully used to investigate the propagation of the Indian Ocean Kelvin waves in the Indonesian seas (Yuan et al., 2018), the dynamics of the North Equatorial Subsurface Current (X. Li et al., 2020), and the interannual variability of the Lower Equatorial Intermediate Current (Ma et al., 2020). The LCSM is configured for the whole tropical Indo-Pacific Oceans from 30°S to 30°N, 30°E to 60°W, with a horizontal resolution of 0.1° to resolve the straits and islands in the Indonesian seas. The ETOPO1 200 m isobath is used to set the land mask of the model. There are 50 vertical modes in the model based on the background density profile following Yuan et al. (2018). The first 10 baroclinic modes are summed as the total solution in this study. Same as the PIOM simulation, the LCSM is integrated for 30 years from 1990 forced by the same NCDC blended wind data, and the results from year 2000–2016 are used to compare with the PIOM simulation.

# 3. Interannual Variability in the Indonesian Seas

## 3.1. Model Validation

Liang et al. (2019) provided a preliminary evaluation of the PIOM simulated sea surface height (SSH) forced by the monthly climatological wind, and found the model simulates quite well not only the pattern but also the magnitude of the SSH over the whole domain. In this study, we first validate the sea level variability in the Indonesian seas from the 17-year PIOM real-time simulation output from 2000 to 2016 using the AVISO sea level data.

Considering the different reference sea levels used in the satellite altimetry and model, we choose to compare the empirical orthogonal function (EOF) modes for the interannual variability of SLA instead of comparing the SLA directly. The EOF analysis is conducted for a subdomain in the western Pacific and Indonesian Seas (15°S to 15°N, 100° to 150°E). Figure 1 shows the comparisons of the pattern and principal components of the first EOF mode, which accounts for 61% and 39% of the SLA variances in AVISO data set and model simulation,

respectively (Figure 1e). The simulated and observed EOF patterns show quite similar distributions of sea level anomaly from the western Pacific Ocean to the eastern Indian Ocean via the Indonesian seas (Figures 1a and 1b). Compared to the observation, the model seems to overpredict the oceanic connection between the Indo-Pacific Oceans through the eastern Indonesian seas and underpredict along the western pathway, as the simulated SLA anomalies are larger in the Halmahera and Banda Seas but smaller in the Sulawesi Sea and Makassar Strait than those in the observation (Figure 1c). Negative anomalies during the El Niño years (or positive anomalies during the La Niña years, according to the principal components in Figure 1d) in the western Pacific is centered along 5°N between 127°E and 140°E approximately in both observation and simulation, except there is a secondary anomaly at 10°N in AVISO, which is notably weaker in the model (negative differences along 10°N in Figure 1c). Besides, there remains differences in the SLA gradient along the south Java coast and in the west Banda Sea where the model overestimates the SLA gradients in the offshore direction compared with those in the observation (positive differences in Figure 1c).

The corresponding principal components (PCs) of the first mode are compared in Figure 1d. The simulated SLA variability coincides approximately with the observation. Both PCs show high correlation with the Niño 3.4 Index with a correlation coefficient of 0.82 for AVISO and 0.76 for PIOM (the 95% significance level is at 0.44 and 0.42 with an effective degree of freedom of 18 and 20, respectively), which indicates the first mode is highly related to ENSO. However, the response to ENSO in the model is weaker than that in the observation, as the comparison of the percent variance of this mode reflects in Figure 1e. Overall, the sea level variability in the Indonesian seas is successfully simulated by the PIOM regional ocean model as compared with AVISO altimeter observation, except the ENSO signal in the model is somewhat weaker.

Observations of the ITF in the Indonesian Seas have been increased since 2000s owing to various international observation programs. In this section, we compare the simulated velocity in the Makassar Strait and in the Halmahera Sea with the mooring observations. The model velocity is selected at the nearest grid point to the mooring locations. The results are presented in Figure 2 for the meridional velocity in the Makassar Strait, and in Figure 3 for the along strait velocity (ASV) in the Halmahera Sea. The ASV is calculated along the direction of 20° clockwise from due north, following X. Li et al. (2020). Both the observed and simulated meridional velocity in the Makassar Strait show strong southward Makassar throughflow above 600 m depth, and northward velocity in deeper layers (Figure 2), which is regarded as the main part of ITF (Gordon et al., 2010). The maximum value of the southward velocity in PIOM simulation is about  $1.21 \text{ m s}^{-1}$ , which compares favorably with the observation ( $1.23 \text{ m s}^{-1}$ ). However, the strongest southward currents in the observation are located at about 100 m, while in the model they occur at ~150 m. Moreover, the observed velocities decay rapidly in the depth range from 100 to 400 m, whereas the modeled southward throughflow remains relatively strong in the upper 500 m, hence relatively large differences between the observation and the simulation can be seen below the 200 m depth (the red curve in Figure 2c).

The ASV in the Halmahera Sea shows strong annual cycle during the period of observation from November 2015 to October 2017, which is successfully simulated by the model especially in the timing of the seasonal shifts (Figures 3a and 3b). Both the modeled and observed ASVs show northeastward velocity (positive ASV) from December to April, and southwestward velocity (negative ASV) in summer and fall seasons in the upper layer above 200 m, together with reversed phases below this depth. However, the model overestimates the northeastward velocity and underestimates the southwestward velocity in the upper layer, which results in opposite time averaged ASVs and the biggest difference in the vertical profile (Figure 3c). Below 200 m, the simulated ASVs are stronger in both directions than the observed ASVs. The maximum time averaged ASV below 200 m in the model is twice larger than that in the observation, at about 550 m (Figure 3c). There is no big difference between observed and simulated ASVs between 800 and 1,000 m depths.

### 3.2. Interannual Variability of the Sea Level

We examine the interannual variability of SLA in the Indonesian seas in this section using the PIOM simulation and observational sea level products. Figures 4a–4c show the interannual sea level anomalies averaged in the inflow passages of ITF: the Sulawesi Sea basin (2°–5°N, 121°–124°E) (Figure 4a), the Halmahera Sea (2°S–0°, 128°–130°E) (Figure 4b), and the Makassar Strait (3°–1°S, 117°–119°E) (Figure 4c). The three areas are marked in black boxes in Figure 1a, and the anomalies are obtained by subtracting the climatological seasonal cycles derived from 2000 through 2016 (Figure S1 in Supporting Information S1). It is clear that the SLA attains

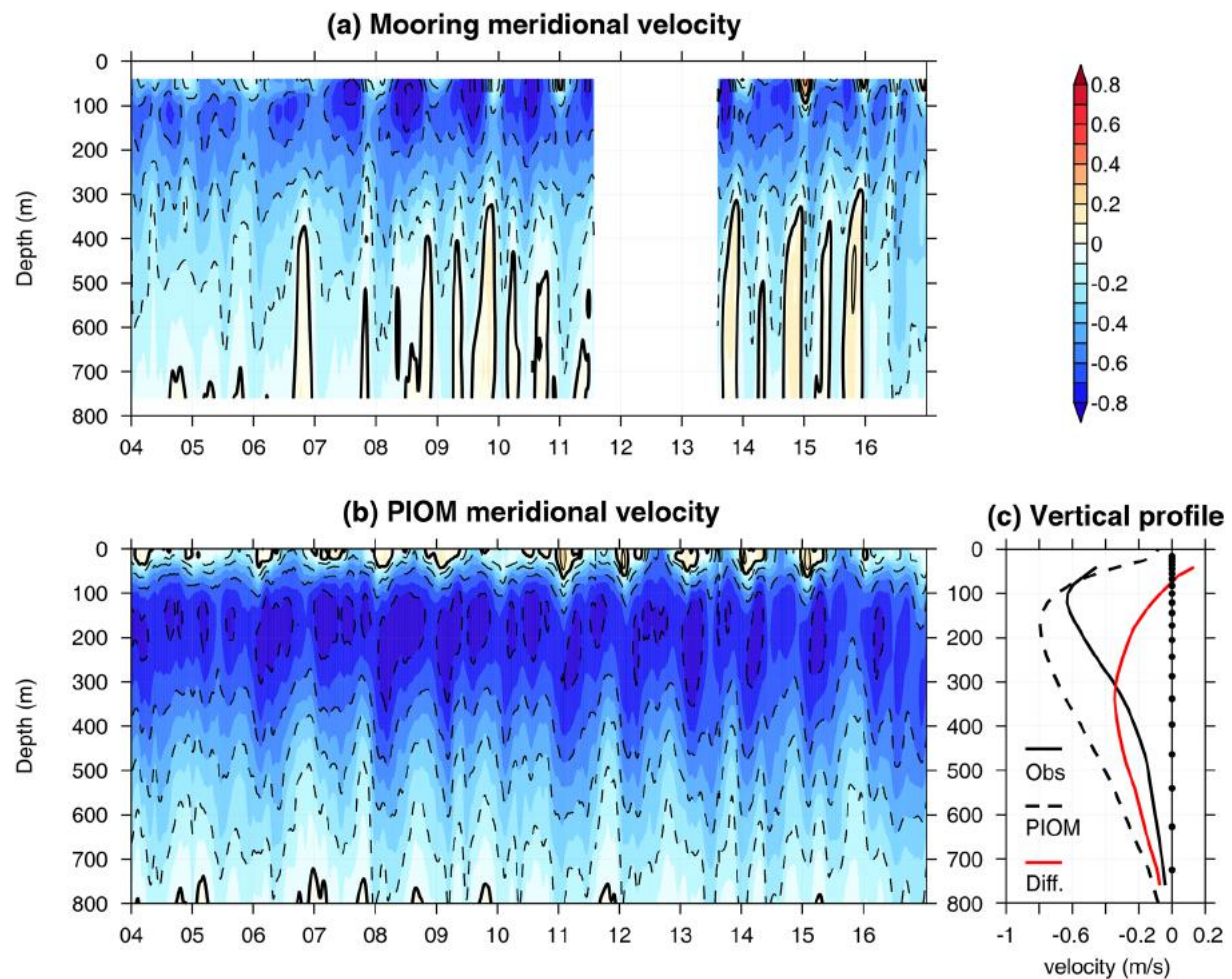


**Figure 2.** The 120-day low-pass filtered daily meridional current ( $\text{m s}^{-1}$ ) observed by the Makassar Strait moorings (a) and simulated by PIOM model (b). Panel (c) shows time-averaged vertical profile of the velocities ( $\text{m s}^{-1}$ ) and the difference between them (red curve). The contour intervals are  $0.2 \text{ m s}^{-1}$  in (a) and (b). Black dots along the zero-gridline in (c) indicate the vertical layers of PIOM model.

positive (negative) anomalies during the cold (warm) phase of ENSO in both the observation and model simulation. The PIOM simulated and the observed SLA agree with each other very well, with correlation coefficients all above the 95% significance level (at 0.58 with an effective degree of freedom of 10). The simulation slightly underestimates the observation, especially during the years from 2002 to 2004 and from mid-2007 to mid-2009 for the Sulawesi Sea. It is compared very well with the AVISO SLA in the Halmahera Sea, except for a discrepancy of about 5 cm during the 2015/2016 super ENSO event (Figure 4b). These differences may be due to the different spatial resolutions of model and satellite products, especially in areas heavily affected by adjacent lands like this region.

The lag correlations between interannual SLA and wind anomaly averaged in the same three regions show insignificant correlations at zero-month lag in both zonal and meridional wind directions (Figures 4d–4f). The highest correlations with the meridional wind appear at a time lag of about four to six months (blue curves in Figures 4d–4f), while those with the zonal wind appear at a time lag of about four months in the Sulawesi Sea (red curves in Figure 4d) and eight months in the Halmahera Sea (red curves in Figure 4e). These results suggest the interannual signals in the SLA could not be driven by the local forcing. Instead, the ENSO-related interannual SLA variation could be forced by the remote interannual oscillations from the Pacific Ocean, which is further analyzed in Section 4 below.

To have a better understanding of the sea level variations on specific interannual period in the western and eastern ITF inflow passages, we performed the ensemble empirical mode decomposition (EEMD) analysis on the SLA



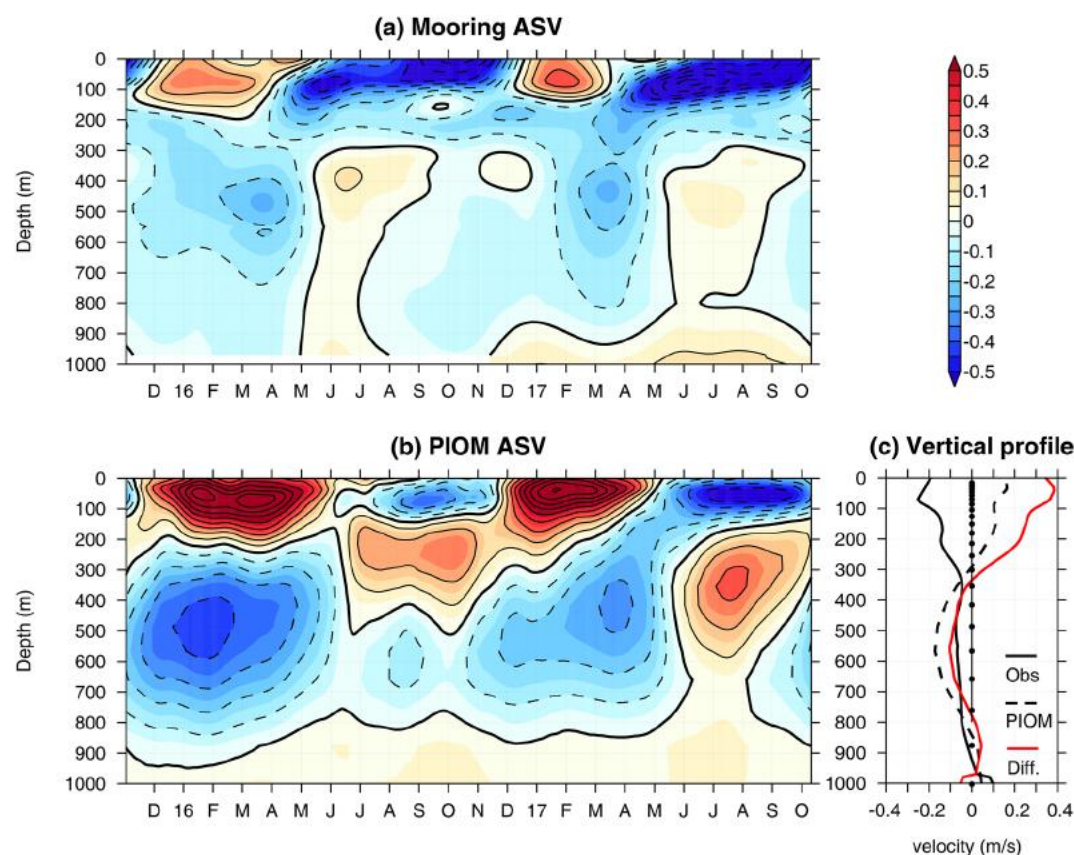


**Figure 3.** Same as Figure 2 but for the 120-day low-pass filtered daily ASV observed by the Jailolo Strait mooring in the Halmahera Sea.

averaged in the Sulawesi Sea and the Halmahera Sea (see the black boxes in Figure 1a), which could be regarded as the entrance of the western and eastern passages, respectively (Figure 5). The EEMD method used in this study is from Wu and Huang (2009) and has been successfully applied in oceanographic research (e.g., Palacz et al., 2011). This method decomposes data series into intrinsic mode functions (IMFs) with different frequencies, and a residual trend. Thus, the true variabilities of the data in various periods can be studied separately. Parameters for EEMD follow those of Palacz et al. (2011) with 0.2 for An (the amplitude of added white noise) and 600 for Nesb (the number of ensembles), respectively.

In this study, we classified IMFs C3 and C4 with periods ranging from three to five years as the interannual variability according to the IMFs' statistical significance (Figure S2 in Supporting Information S1). As expected, the sum of C3 and C4 for the SLA in the Halmahera Sea appears to have almost the same variation as Niño 3.4 in both AVISO observation and PIOM simulation, with correlation coefficient of 0.53 and 0.75, respectively (the 95% significance level is at 0.38 and 0.40), indicating the dominance of ENSO signals in this passage (blue curves in Figures 5a and 5b). For the SLA oscillations in the Sulawesi Sea, the results show a mixing of the seasonal signal, especially from 2011 to 2013 in the observation (red curves in Figure 5a). However, the ENSO-related interannual signal is also significant in the Sulawesi Sea. The correlation coefficient is 0.52 for AVISO and 0.78 for PIOM, with the 95% significance level at 0.30 and 0.27.

IMFs C5 and C6 (periods from six to eight years) also account for considerable amount of the total variability in both seas and statistically significant. The sum of C5 and C6 follows a longer period modulation to the Niño index (Figures 5c and 5d), which is probably dominated by the low frequency oscillation such as the Pacific Decadal Oscillation (PDO). In particular, the positive PDO index lasting from 2002 to 2005 and the negative PDO index from 2008 to 2013 are significantly correlated with the positive and negative anomalies in C5 + C6. Therefore, the interannual or lower-frequency variations in SLA in both the Sulawesi Sea and the Halmahera Sea are likely driven by climate signals from the Pacific Ocean.

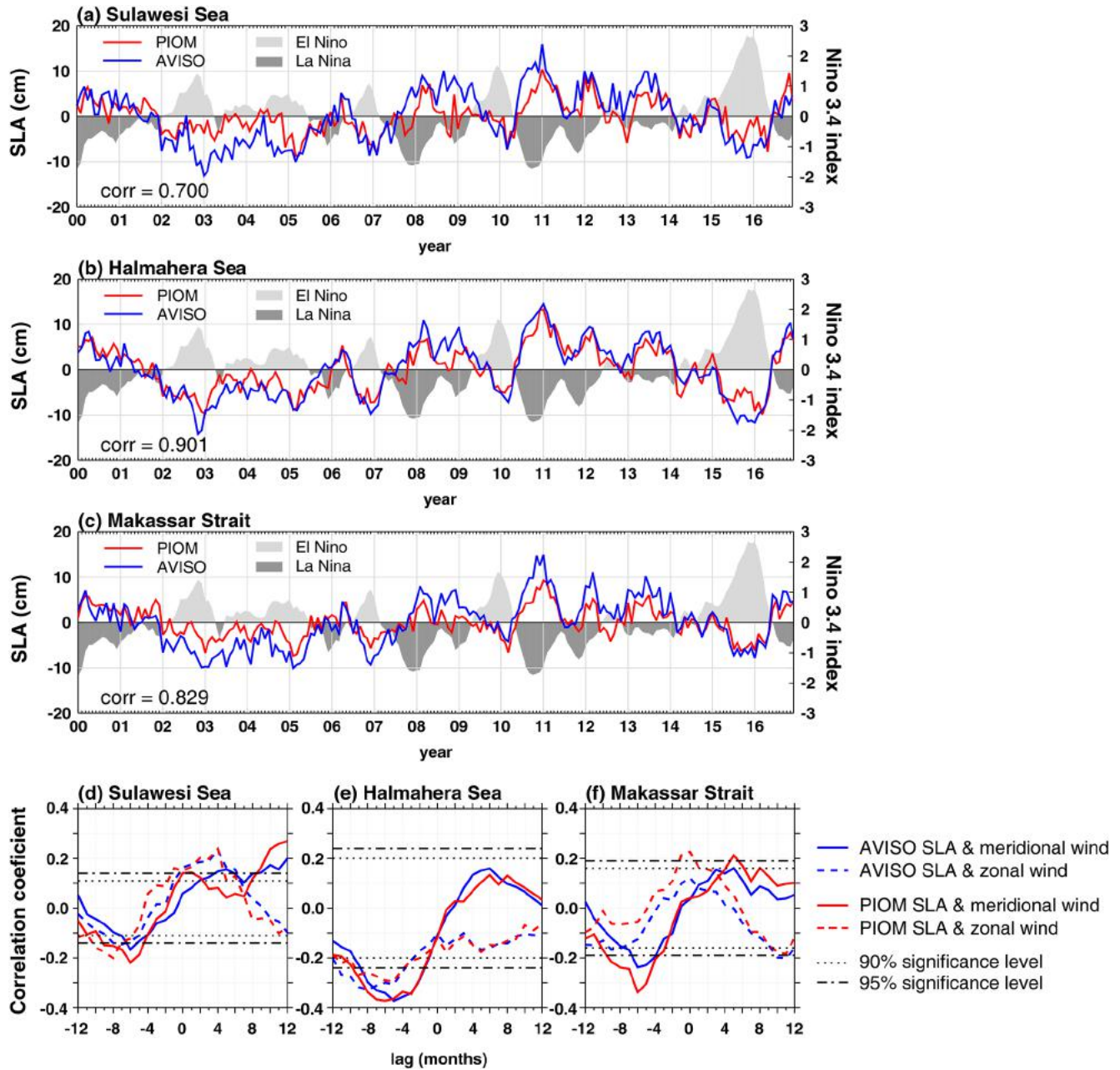


**Figure 4.** Interannual SLA variability (cm) averaged in the (a) Sulawesi Sea, (b) the Halmahera Sea, and (c) the Makassar Strait from 2000 to 2016 using AVISO observation (blue curves) and PIOM simulation (red curves). The average areas are shown as the black boxes in Figure 1a. Panels (d–f) are the lag correlations between SLA and local winds averaged in the same areas. Shadows in (a–c) represent the Niño 3.4 index. Dotted and dot-dashed lines in (d) to (f) represent the 90% and 95% significance levels, respectively.

### 3.3. Interannual Variability of ITF in the Makassar Strait and Halmahera Sea

To investigate the interannual variability of local winds and ITF in the Makassar Strait and Halmahera Sea are investigated, we use the velocities at the same grid points as in Figures 2 and 3 to represent the simulated ITF in the Makassar Strait and the Halmahera Sea, and the local wind calculated from the daily NCDC blended wind as the average in a  $1^\circ \times 1^\circ$  box around the model grid points. Since the meridional velocity is used for the ITF in the Makassar Strait and the ASV for the Halmahera Sea location is along the direction of  $20^\circ$  from due north, only the meridional local winds are shown (Figures 6a and 6b). As we do for calculating the interannual sea level variation, the climatological seasonal cycles during 2000–2016 are removed to obtain the interannual variability



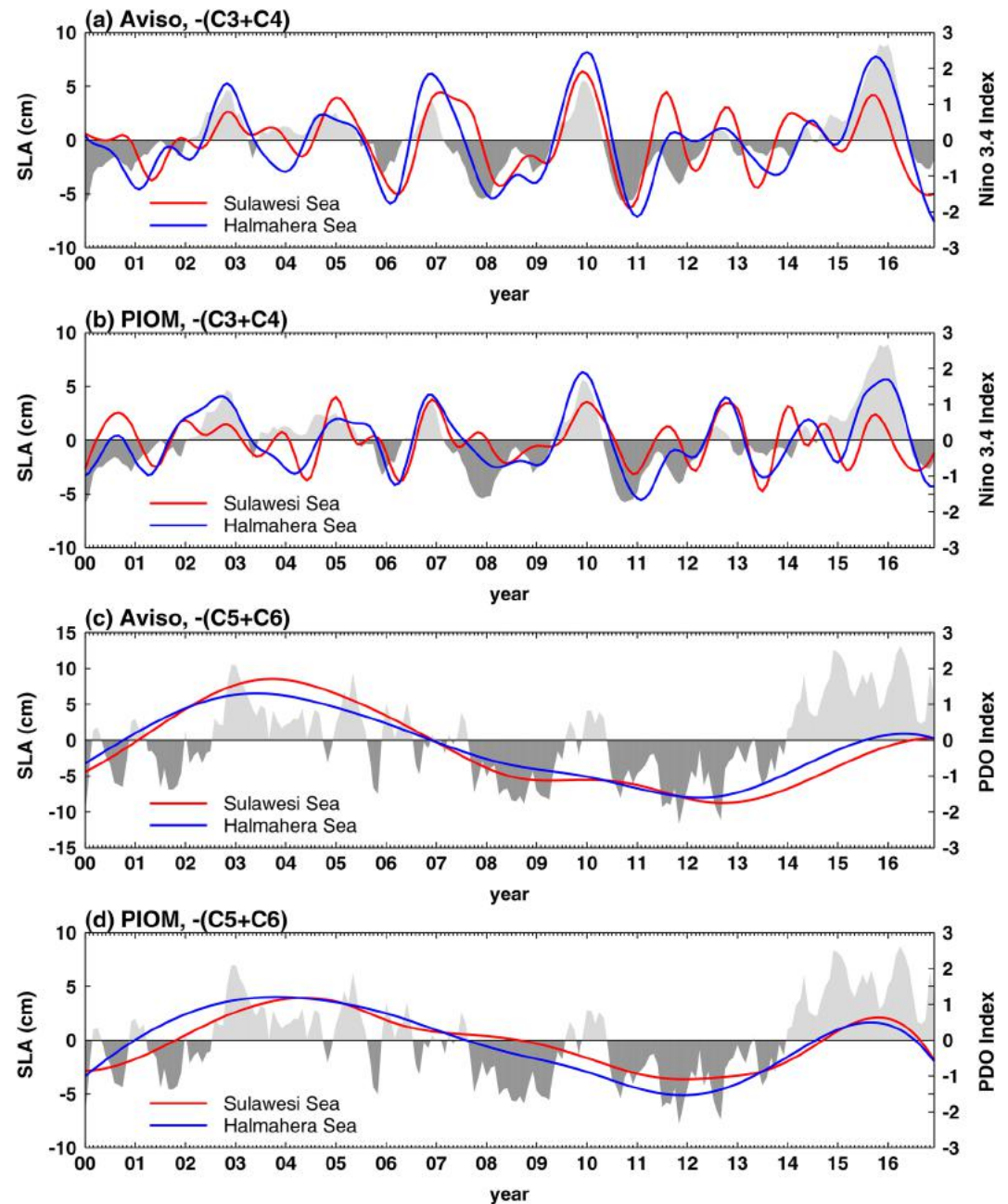


**Figure 5.** (a and b) Combined interannual and (c and d) low frequency oscillations from the EEMD analysis performed on the averaged SLA (cm) in the Sulawesi Sea (red curves) and Halmahera Sea (blue curves) using (a and c) AVISO observation and (b and d) PIOM simulation. Shadows represent the Niño 3.4 index in (a and b) and PDO index in (c and d), respectively.

of the wind and currents. The interannual variabilities of the local winds in both straits are much smaller than their seasonal cycles, that is, monsoon winds (Figure S3 in Supporting Information S1), which suggests seasonal variability dominates. The results show similar interannual variability between the local winds at both locations, which lead the Niño 3.4 by about three to four months, with northward anomalies during El Niño events and southward anomalies during most of La Niña events.

It is interesting that the velocities in the Makassar Strait and Halmahera Sea reveal opposite anomalies vertically at the interannual time scales (Figures 6c and 6d). In the Makassar Strait the surface current is in the direction of local wind for most of the time except for periods during 2006–2007, 2012–2013, and the second half of 2016 (Figure 6a), while in the Halmahera Sea the surface current is mostly in the direction opposite to the

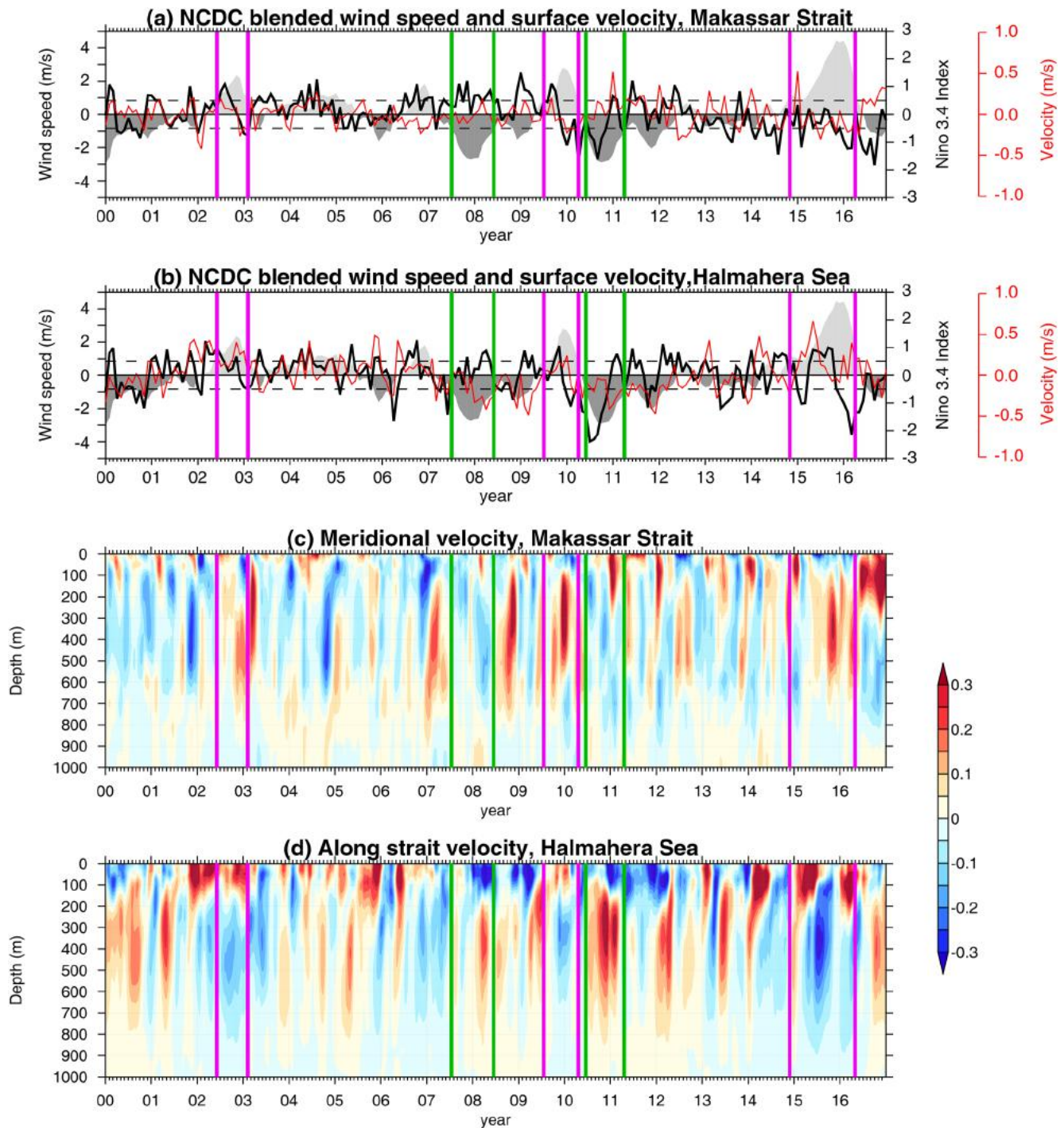


**Figure 6.** The 120-day low-pass filtered interannual daily meridional winds ( $\text{m s}^{-1}$ ) and simulated surface meridional velocity ( $\text{m s}^{-1}$ ) averaged in upper 50 m in the Makassar Strait (a) and the Halmahera Sea (b), the simulated interannual variability of the meridional velocity ( $\text{m s}^{-1}$ ) at the Makassar Strait mooring site (c), the simulated interannual variability of the along strait velocity ( $\text{m s}^{-1}$ ) at the Halmahera Sea mooring site (d). Shadows in (a) and (b) represent the Nino 3.4 index. Dashed lines in (a) and (b) indicate the index of  $\pm 0.5$ . Green and pink boxes mark the La Niña and El Niño periods, respectively.

local wind during ENSO events (Figure 6b). The model shows southward and northward anomalies in the top 100 m in the Makassar Strait during El Niño and La Niña events, respectively, while the velocity anomalies are reversed between 100 and 700 m. In particular, the model successfully captured the exceptionally large decline of the velocity in the upper 300 m during the summer of 2016 reported by Pujiana et al. (2019) as well as the

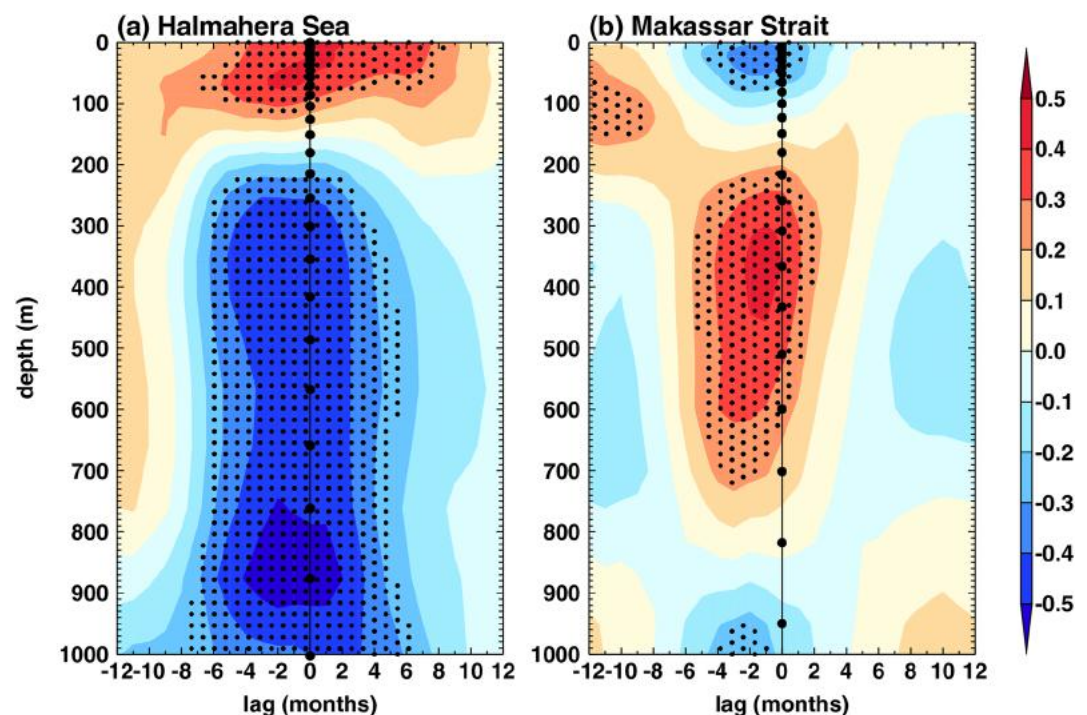


**Figure 7.** The lag correlations between Niño 3.4 index and the PIOM simulated meridional current profiles in the Halmahera Sea (a) and the Makassar Strait (b). Dotted shadings indicate correlations above the 95% significance level. Black dots along the zero grid lines indicate the vertical layers of the PIOM model.

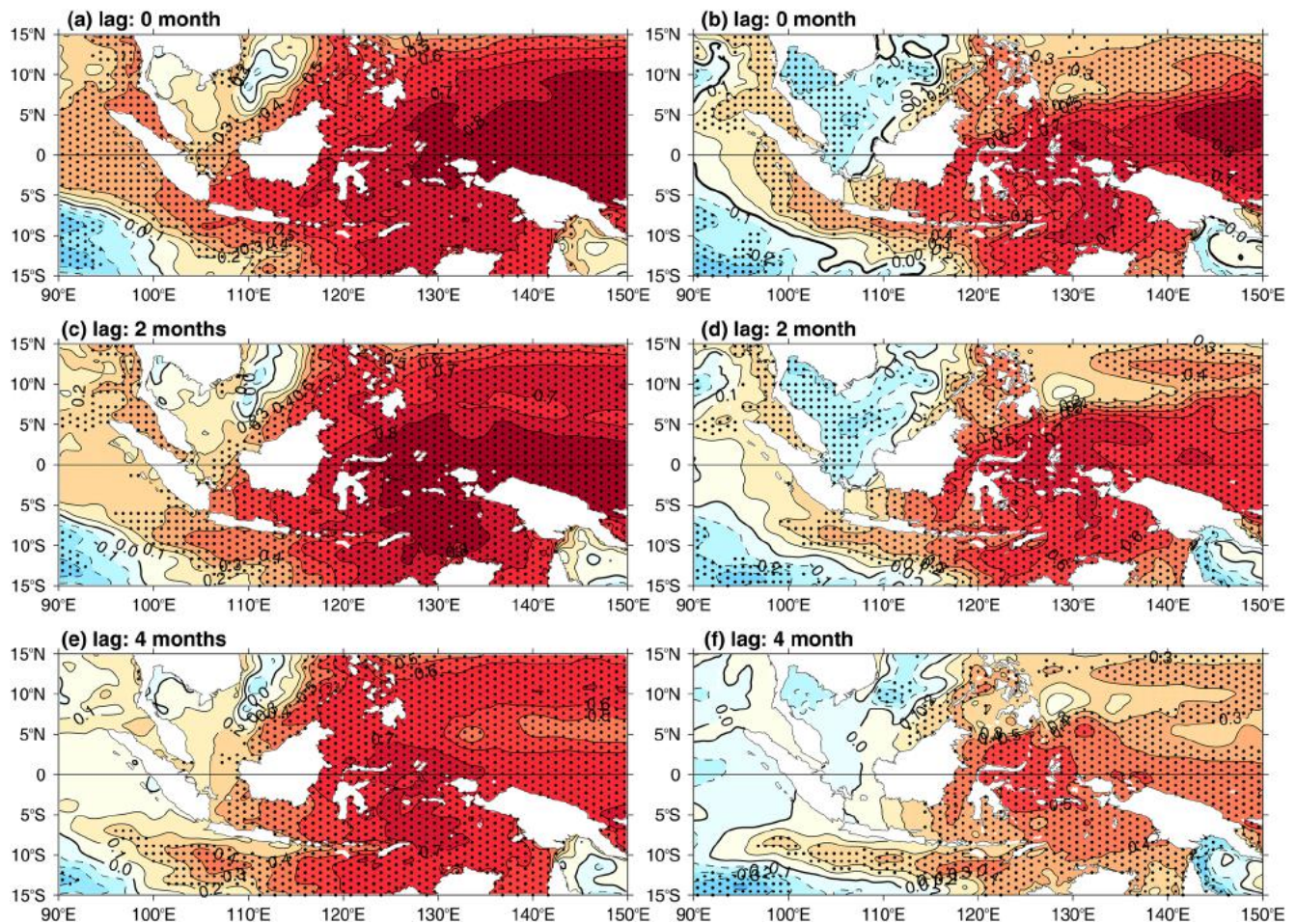
strengthening of the sub-thermocline velocity during 2008 and the summer of 2016, similar to the findings of Gordon et al. (2012) and M. Li, Yuan, et al. (2021). On the contrary, the ASV in the Halmahera Sea presents pronounced northward (southward) anomalies during El Niño and southward (northward) anomaly during La Niña at depths from 0 to 200 m (200–700 m), respectively (Figure 6d). Moreover, the anomalies below the thermocline appear to lead the surface signals at both locations. As a result, the subsurface anomalies lead the local winds by two to three months, implying the anomalies are probably dominated by the remote forcing, like ENSO induced waves from the Pacific Ocean.

Figure 7 shows the lag correlations between the velocity profiles and Niño 3.4 index. Negative time-lags represent the velocities lag the index. The opposite responses between the Makassar Strait and the Halmahera Sea are apparent, as well as the opposite responses above and below the thermocline. Using mooring data, reanalysis and model data, M. Li et al. (2020) found that the ITF inflow responds to ENSO at sub-thermocline in the depth range of 300–760 m. Similar results are also present in the PIOM simulated velocities. The lag correlations show maximum significant correlation at time-lags of 2–4 months in depths between 300 and 700 m in the Makassar Strait, and at about 1 month in depths below 300 m in the Halmahera Sea (Figure 7). The northward (southward) anomalies of the meridional velocity in the sub-thermocline in the Makassar Strait during El Niño (La Niña) and opposite anomalies of the ASV in the Halmahera Sea are correlated with ENSO at time-lags of several months, indicating the propagation of the ENSO signal in both pathways in the Indonesian seas. Furthermore, the opposite anomalies in the two pathways may be associated with pathway-specific differences in transmitting the ENSO signal during different ENSO phases, which will be discussed in detail in the next section.

#### 4. Propagation of Interannual Anomalies Into the Indonesian Seas

The evident correlations between the interannual SLA/velocity and the ENSO index illustrated in Section 3 suggest potential responses to Pacific ENSO signals in both the eastern and the western passage of ITF in the Indonesian seas. In this section, we try to identify the pathways for the ENSO signal to affect the SLA in these passages during different ENSO phases and the associated dynamics.





**Figure 8.** The correlation coefficients between the interannual sea level anomalies averaged in ( $2^{\circ}$ – $6^{\circ}$ N,  $145^{\circ}$ – $155^{\circ}$ E) and the eastern Indian Ocean-western Pacific Ocean basin observed by AVISO altimetry (left column) and simulated by PIOM (right column) with a time lag of 0, 2, and 4 months. Dotted shadings indicate correlations above the 95% significance level.

#### 4.1. Sources of the Interannual Signal From the Pacific Ocean

Considering the largest amplitude of the equatorial Rossby wave is located between  $2^{\circ}$  and  $6^{\circ}$ N according to the meridional structure in the linear equatorial wave theory (Boulanger & Menkes, 1995), we choose the area from  $2^{\circ}$  to  $6^{\circ}$ N at the western Pacific centered at  $150^{\circ}$ E as the equatorial SLA source. Figure 8 shows the lag correlations between the interannual equatorial SLA of the western Pacific Ocean and the eastern Indian-western Pacific SLA with time lags of 0, 2, and 4 months in both simulation and observation. The lag correlations observed by the satellite altimeter show high correlation above 95% significance level in most of the Indonesian seas and western Pacific basins (Figures 8a, 8c, and 8e), while the high correlation in the PIOM simulation centered between  $5^{\circ}$ N and  $5^{\circ}$ S (Figures 8b, 8d, and 8f). Both results indicate a pronounced westward propagation of the highest correlation, from the equatorial Pacific Ocean to the Indonesian seas. This suggests a Rossby wave propagation in transferring the ENSO signal. The high correlations in the Indonesian seas span across the Sulawesi Sea then the Makassar Strait and the eastern Indonesian seas (Figures 8c and 8d), and finally into the Indian Ocean (Figures 8e and 8f), which implies both pathways for the Pacific Ocean interannual signal to influence the SLA in the Indonesian seas, and further, the Indian Ocean.

Waters from both the Northern and Southern Hemispheres in the Pacific Ocean form the ITF via the ensemble of Pacific western boundary currents (D. Hu et al., 2015). Thus, not only the ENSO signal originated from the equatorial Pacific Ocean may propagate into the Indonesian seas, interannual variations in off-equator areas may also enter and modulate the interannual anomaly within the passages of the ITF. Lag correlations between the interannual SLA in the northwestern ( $10^{\circ}$ – $20^{\circ}$ N,  $145^{\circ}$ – $155^{\circ}$ E) and southwestern ( $20^{\circ}$ – $10^{\circ}$ S,  $145^{\circ}$ – $155^{\circ}$ E) Pacific

**Table 1**  
*The Transmission Rates (%) at the Western (Sulawesi Sea) and Eastern (Halmahera Sea) Passages During the El Niño and La Niña Events From 2000 to 2016*

	Event	Period	Sulawesi Sea AVISO/ PIOM	Halmahera Sea AVISO/ PIOM
El Niño events	2002/2003	2002-05 to 2003-03	51.2/19.4	54.5/56.9
	2009/2010	2009-07 to 2010-04	18.5/31.0	39.3/62.1
	2015/2016	2014-10 to 2016-05	40.4/18.9	70.8/55.5
La Niña events	2000/2001	2000-01 to 2001-02	39.0/30.7	39.3/49.2
	2007/2008	2007-07 to 2008-06	46.8/24.4	46.2/37.4
	2010/2011	2010-06 to 2011-05	55.7/31.6	56.1/49.1

along the same longitude range as the equatorial Pacific, and the interannual SLA over the eastern Indian-western Pacific are also examined, respectively (Figures S4 and S5 in Supporting Information S1). The correlations with the SLA in the northwestern Pacific (Figures S4 in Supporting Information S1) are smaller than those in Figure 8, with most of the significant correlations lie in the north of Sulawesi Sea, the Sulu Sea, and around the Philippines, while the correlations with the SLA in the southwestern Pacific Ocean are insignificant in the Indonesian seas in both observation and model simulation (Figure S5 in Supporting Information S1), suggesting the source of the ENSO-related interannual variations in the Indonesian seas is more likely from the equatorial Pacific Ocean. Researches on water mass and current have proven that the water from the south Pacific carried by the New Guinea Coastal Current and New Guinea Coastal Undercurrent can cross the equator to arrive at the Sulawesi Sea (Fine et al., 1994; D. Hu et al., 2015; Lindstrom et al., 1987; Qu & Lindstrom, 2004). However, this process is not significant in the lag correlations of the SLA.

#### 4.2. Propagation of the Oceanic Waves From the Pacific in Different ENSO Phases

Traveling oceanic planetary waves could be important dynamics in carrying and delivering the interannual signals through the Indonesian seas, like the equatorial Rossby waves and coastally trapped Kelvin waves (Drushka et al., 2010; X. Hu et al., 2019; Pujiana et al., 2013; Susanto et al., 2000; J. Wang et al., 2020; Wijffels & Meyers, 2004). Previous studies have verified the westward and downward propagation of the Rossby waves from the Pacific Ocean to the western boundary, and discussed the waveguide through the Halmahera Sea along the Papua-Australia Shelf inside the Indonesian seas (McClellan et al., 2005; Wijffels & Meyers, 2004). However, the ENSO-related interannual variability in the western passages (the Sulawesi Sea and the Makassar Strait) discussed above suggests the possibility of the western waveguide. The two possible waveguides may play different roles in different phases of ENSO. In this section, roles of the western and eastern passages in transmitting the ENSO signal from the western Pacific are investigated, especially during the warm and cold ENSO phases.

To assess the contributions of each waveguide quantitatively, we calculate the ratio of the sea level amplitude at the entrance of the western (the Sulawesi Sea) and the eastern (the Halmahera Sea) pathway to the sea level amplitude in the western Pacific as the transmission rate, respectively. Areas used to obtain the averaged sea level amplitude for the Sulawesi and Halmahera Seas are the same boxes as in Figure 1a, and for the western Pacific a  $2^{\circ} \times 2^{\circ}$  box centered at ( $4^{\circ}\text{N}$ ,  $135^{\circ}\text{E}$ ). The ratios are then averaged as the transmission rates for each El Niño and La Niña events when the Niño 3.4 index is larger than  $0.5^{\circ}\text{C}$  or smaller than  $-0.5^{\circ}\text{C}$  for at least six consecutive months following the definition of the ENSO events by Trenberth (1997). The results are listed in Table 1.

There are three El Niño and three La Niña events during the whole time series from 2000 to 2016 (Table 1). The observations show that the sea level anomaly propagates into the Indonesian seas primarily through the eastern pathway (the Halmahera Sea) during the El Niño events, especially the 2015/2016 event, while during La Niña, the transmission rates of the two pathways are close to 1:1. The highest observed transmission rate during the 2015/2016 event may be related to the strength of ENSO: the SLA anomaly was largest in area and lasted the longest in the eastern Pacific during the 2015/2016 El Niño, making the anomaly in the western Pacific more intense and extensive to intrude the Indonesian seas. The simulated transmission rates at the Halmahera Sea are more than twice of those at the Sulawesi Sea during El Niño, and the rates at the Halmahera Sea decrease significantly while those at the Sulawesi Sea increase slightly during La Niña. The transmission rates are smaller in the simulation especially for the western pathway, which could be due to the underestimation of the western connection in the model as we mentioned before in Section 3.1, but the trends associated with different ENSO phases are similar between the simulation and the observation. In general, for the interannual SLA propagating from the western Pacific into the Indonesian seas, both the AVISO altimeter data and the model show a preference of the eastern pathway (the Halmahera Sea) during El Niño years, while the preference is less pronounced during La Niña years.



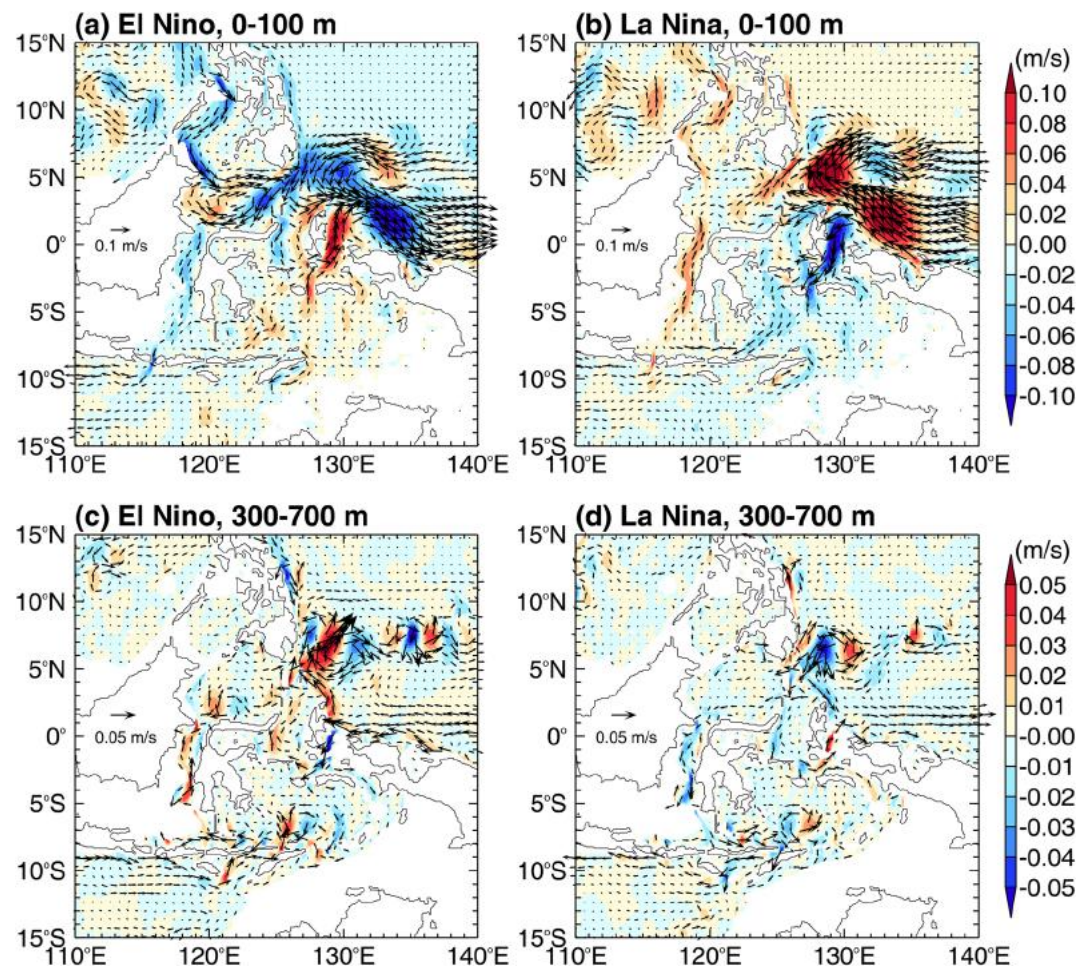


**Figure 9.** The composite interannual currents (vectors,  $\text{m s}^{-1}$ ) averaged above (a and b) 100 m and between (c and d) 300 and 700 m during the (a and c) El Niño and (b and d) La Niña events simulated by PIOM regional model. Color represent the meridional velocity ( $\text{m s}^{-1}$ ): northward anomaly in positive value (red) and southward anomaly in negative value (blue).

### 4.3. Dynamics

#### 4.3.1. Interactions With the WBCs

Located at the western boundary of the Pacific Ocean, the ITF entrance is influenced by the shifting of the WBCs during ENSO phases, and so is the wave propagation in this region. Previous studies have pointed out that the relationship of the interannual variability of WBCs to ENSO (e.g., D. Hu et al., 2015; Kashino et al., 2009, 2013): During El Niños, the North Equatorial Current, the North Equatorial Counter Current (NECC) and the Mindanao Current are enhanced, together with strengthened Mindanao Eddy (ME), weakened Halmahera Eddy, and weakened New Guinea Coastal Current. Responses are the opposite during La Niñas. The anomalous WBCs are successfully simulated by PIOM. Figures 9a and 9b show the composite surface flow field anomaly maps corresponding to the warm and cold ENSO phases, respectively. The ENSO periods for the composites are the same as given in Table 1. In depths above 100 m, the simulated currents show significantly stronger NECC and ME, and the NECC shifted southward during El Niño years (Figure 9a). During La Niña years, the NECC had westward anomaly and the ME became weaker (Figure 9b).

As described in Section 3.3, the sub-thermocline velocities in the Makassar Strait and the Halmahera Sea also respond to ENSO. The composite currents averaged in depths between 300 and 700 m (Figures 9c and 9d) show phases opposite to the currents at the surface with evident anticyclone (cyclone) trains in the western Pacific during El Niño (La Niña) events. The WBCs present a penetrating state into the western waveguide during the cold ENSO phase (Figure 9d), which allows the Rossby waves to propagate westward nearly uninterrupted



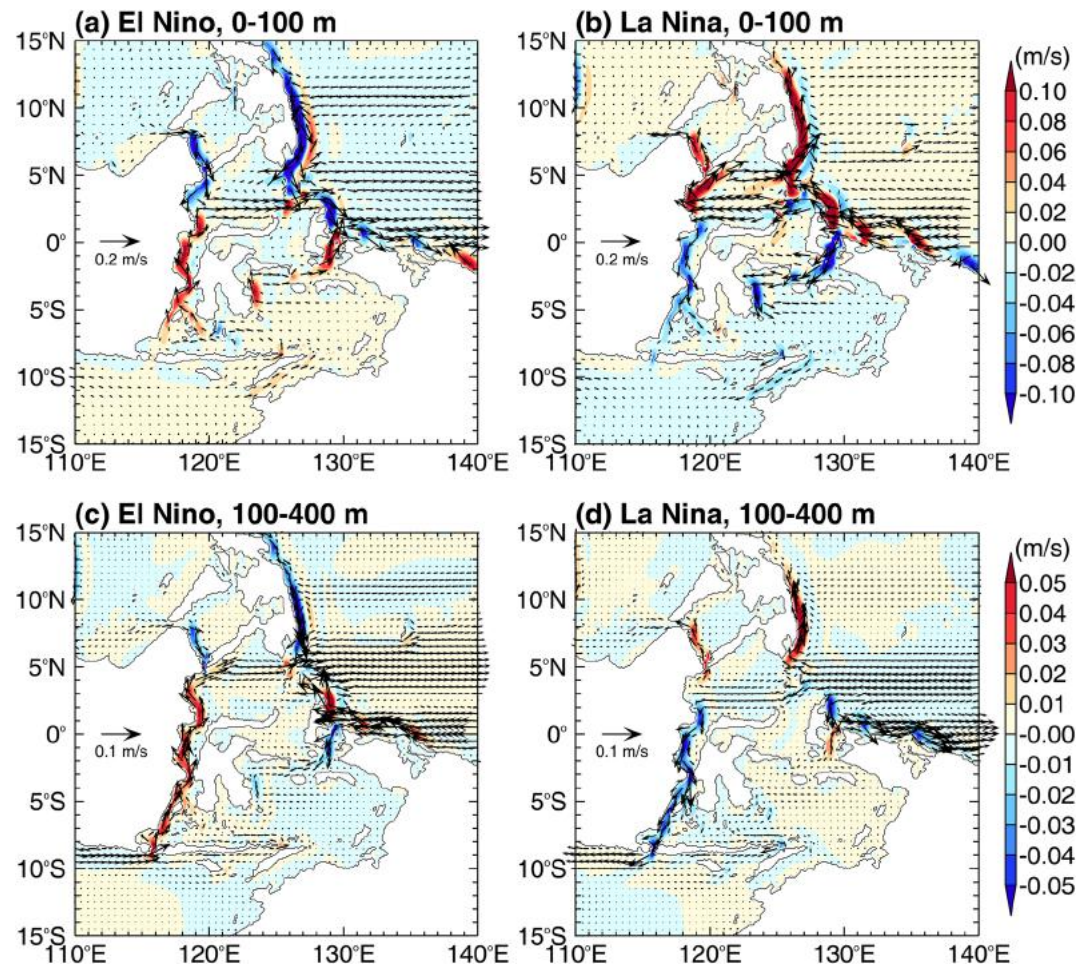


**Figure 10.** Same as Figure 9 but for LCSM.

through the gap in the western boundary and into the western pathway in the Indonesian seas. In comparison, the leaping state of the WBCs at the entrance of the Indonesian seas during the warm ENSO phase (Figure 9c) tends to block the westward propagated ENSO signals according to the nonlinear reflection dynamics. At the same time, the strengthened westward currents along the New Guinea coast also helps to force the Pacific signals to travel through the eastern waveguide.

#### 4.3.2. Linear Dynamics

The current anomaly at the surface and sub-thermocline layers in the Sulawesi and Halmahera seas simulated by LCSM are presented in Figure 10 to compare with the PIOM simulation (see Figure 9). Since the maximum lag correlation between Niño 3.4 index and the current in LCSM is located at about 300 m depth determined by the mean background density profile (figure omitted), the mean flow field averaged between 100 and 400 m depths in LCSM are calculated to compare with the 300–700 m mean flow field in the PIOM simulation.

At the surface, the LCSM flow field shows clear linear reflection in the Sulawesi Sea during both ENSO phases (Figures 10a and 10b), while the PIOM simulation show a typical WBCs looping state during El Niño and leaping state during La Niña (Figures 9a and 9b) in the Sulawesi Sea, resulting from strong nonlinear processes. At sub-thermocline depths, the effects of the nonlinearity become weaker. There are big differences between LCSM and PIOM simulation during El Niños in the southern Sulawesi Sea: the result in PIOM shows strong eddies (Figure 9c) while in LCSM the currents are quite weak (Figure 10c), indicating that the nonlinear dynamics govern the southern Sulawesi Sea in sub-thermocline during El Niño years and probably block some ENSO signals from propagating through the western passage. On the other hand, LCSM simulated sub-thermocline currents during La Niña years show westward currents in the southern Sulawesi Sea similar to the PIOM result

(Figures 9d and 10d), suggesting the Sulawesi Sea is likely controlled by linear processes during the cold ENSO phase.

In the Halmahera Sea, both the linear and regional models show northward current anomaly during El Niño years and southward anomaly during La Niña years in the surface layer, together with opposite anomalies in the sub-thermocline layers (Figures 9 and 10). Currents along the adjacent New Guinea coast and northern Halmahera Island are also approximately the same in the two models. The consistent flow fields indicate that the ocean dynamics in the Halmahera Sea may be intrinsically nonlinear but rather weak: First, during El Niño events, the New Guinea coast current anomalies are to the south, reducing the strength of the WBC so that more Rossby waves can propagate through the Halmahera Sea, and vice versa during the La Niña events; second, in contrast to the Sulawesi Sea, the opening of the Halmahera Sea is not wide compared to the equatorial deformation radius of the first baroclinic mode.

## 5. Discussions

### 5.1. Propagation of Coastal Kelvin Waves in the Indonesian Seas

Determining waveguides for the coastal Kelvin waves inside the Indonesian seas is a challenging problem due to the fast propagation of the Kelvin waves and complex topography of the Indonesian archipelago. Although the waveguide in the eastern Indonesian seas through the Halmahera Sea—Papuan/Australian shelf has already been proposed (Wijffels & Meyers, 2004, the solid blue arrow in Figure S6 of Supporting Information S1), how the interannual signals in the Sulawesi Sea - Makassar Strait propagate to the Indian Ocean is still a question. Considered the lag correlation in Figure 8 and theory of the coastally trapped Kelvin wave, a probable path is that the Kelvin waves propagate southward along the western edge of the Sulawesi Sea, with the boundary on the right of the propagation direction in the northern hemisphere. After they arrive at the equator, the coastal Kelvin waves would become the equatorial Kelvin waves, and propagate to the east and hit the Sulawesi Island. Then the Kelvin waves continue to propagate as the coastally trapped Kelvin waves with the coast on the left in the southern hemisphere. After that, we suggest there could be two possible waveguides: one is to propagate around the Sulawesi Island through the Banda Sea, where it joins the eastern waveguide; the other is to dash into the Lombok Strait directly as a jet from the Makassar Strait (dashed blue arrows in Figure S6 of Supporting Information S1). Propagation through the western waveguide should be investigated further in the future.

### 5.2. Impacts of Interannual Variability From the Indian Ocean

The velocities in the Makassar Strait as well as in the outflow passages of ITF also correlate with the interannual variability in the Indian Ocean (e.g., Gordon et al., 2019; M. Li et al., 2020; Sprintall et al., 2019). Similar to Figure 8, we also calculate the correlation coefficients between the interannual sea level anomalies averaged in the equatorial eastern Indian Ocean (5°S to 5°N, 80° to 90°E) and the eastern Indian-western Pacific Ocean basin based on satellite altimetry observations (left column) and PIOM simulation (right column) with a time lag of 1, 2, and 3 months, respectively (Figure 11). The results show a tongue of significant correlations along the Sumatra-Java coast, which extends into the Indonesian seas and reaches the Makassar Strait in the observation. The core areas of high correlation are well captured by the PIOM but with smaller magnitude similar to the signals from the Pacific Ocean (Figure 8).

Compared to the significant correlations using the Niño index (see Figure 7a), the correlations between the Dipole Mode Index (DMI), wind, and SLA from the Indian Ocean and the velocity profile in the Halmahera Sea show either insignificant correlation or much smaller correlations at zero lag (Figure 12a and Figure S7 in Supporting Information S1). Thus, we think the influence of the Indian Ocean in the Halmahera Sea could be ignored in this study. On the other hand, DMI, wind, or SLA from the Indian Ocean and the velocity profile in the Makassar Strait all have significant correlations in the sub-thermocline at time lags of 2–4 months, albeit smaller values compared with their counterparts using the Niño index, SLA, or wind from the Pacific Ocean (Figure 12b and Figure S7 in Supporting Information S1). To separate the forcing from the two oceans, the lead author once used an analytical wave model to integrate the wind stress in specific areas along the Kelvin wave characteristics (X. Hu et al., 2019), but this method cannot be applied to predict the velocity profile. However, as discussed by M. Li et al. (2020), forcing from the Indian Ocean wind weakens the effects of ENSO on the ITF. If the contributions of the Indian Ocean were removed, the responses in the Makassar Strait might be strengthened. X. Hu



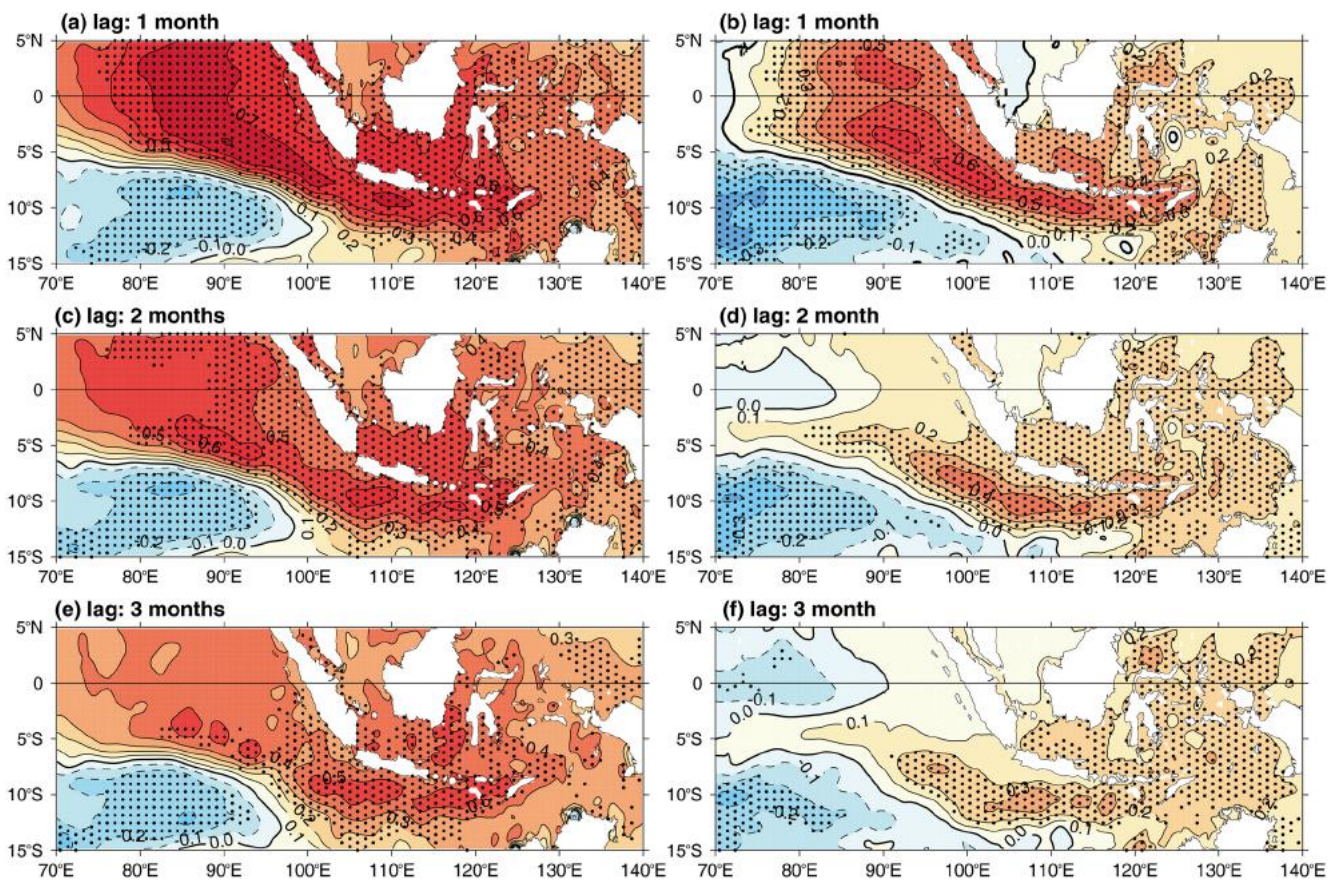


**Figure 11.** The correlation coefficients between the interannual sea level anomalies averaged in (5°S–5°N, 80°–90°E) and the eastern Indian Ocean-western Pacific Ocean basin observed by AVISO altimetry (left column) and simulated by PIOM (right column) with a time lag of 1, 2, and 3 months. Dotted shadings indicate correlations above the 95% significance level.

et al. (2019) also illustrated that the Indian Ocean interannual Kelvin waves influenced the Maluku Channel through the Makassar Strait and Sulawesi Sea during the 2015/2016 El Niño. The preference of Pacific ENSO signals to the eastern passage during the El Niño events could be another mechanism favoring the propagation of the interannual signal from the Indian Ocean in the western pathway. Detailed processes of interactions between the interannual signals from both the Pacific and the Indian Oceans through the Indonesian seas need to be carefully investigated in the future.

## 6. Summary

In this study, we investigate the propagation of the Pacific ENSO signals at entrance of the Indonesian seas using observations and a regional model. The model successfully simulates the interannual sea level variations at the Pacific entrances of the Indonesian seas compared to the AVISO altimeter product, and represents the velocity profiles observed by the moorings deployed in the Makassar Strait and Halmahera Sea. The EOF and EEMD analyses show significant correlations between ENSO index and SLA at both the western and eastern passages of the ITF, as well as the interannual anomalies of the velocities, indicating possible waveguides of the ENSO signals propagation through both pathways.

Lag correlation analyses show the interannual signals at the entrance of the ITF are mainly from the equatorial Pacific Ocean. The equatorial Rossby waves propagate westward and transmit the ENSO-related interannual variability across the western boundary and into the Indonesian seas. Beside of the propagation through the Halmahera Sea - Papuan/Australian shelf (eastern passage) as the coastally trapped Kelvin waves, we find the waveguide through the western passage, the Sulawesi Sea and the Makassar Strait, is also significant in both the observation and model simulation. The composite analysis shows that during the warm ENSO phase (El Niño events), SLA



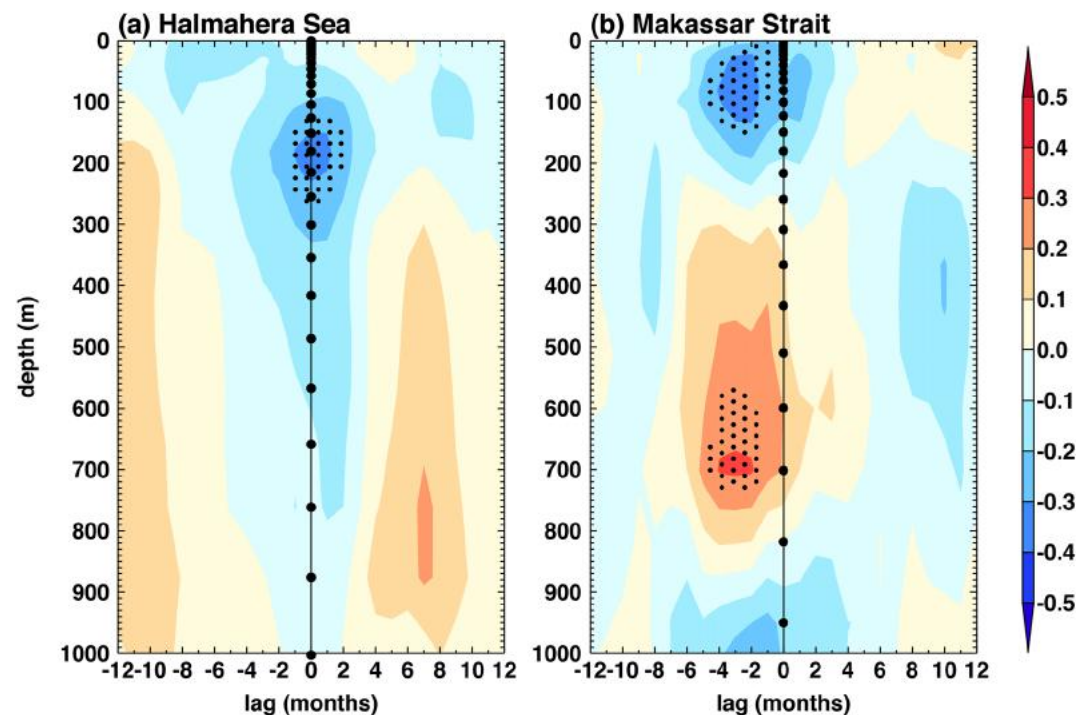


**Figure 12.** The lag correlations between DMI and the PIOM simulated meridional current profiles in the (a) Halmahera Sea and the (b) Makassar Strait. Dotted shadings indicate correlations above the 95% significance level. Black dots along the zero grid lines indicate the vertical layers of the PIOM model.

traveling through the eastern passage are twice stronger than those through the western passage; while during the cold ENSO phase (La Niña events), SLA into the western passage increase, and the transmission rates become close to those in the eastern passage.

The different roles of the western and eastern passages in transmitting the ENSO signals into the Indonesian seas during different ENSO phases may be associated with the penetrating and leaping states of the WBCs, which determine the propagation of the Rossby waves into the Indonesian seas through the western boundary. Besides, the anomalously strong nonlinear ocean processes in the southern Sulawesi Sea during El Niño events further inhibit the ENSO signals from propagating westward. Further studies of these ENSO signals especially how they propagate specifically inside the Indonesian seas and how they interact with the interannual variability from the Indian Ocean in the ITF passages are needed to form a more comprehensive understanding of the climate anomalies in the Indonesian seas.

### Data Availability Statement

The output of the PIOM ocean model and LCSM used in the manuscript can be accessed through [https://pan.baidu.com/s/1z7j-2qqiscQmAEil\\_ZjLFg](https://pan.baidu.com/s/1z7j-2qqiscQmAEil_ZjLFg) with password m750. The mooring data in the Makassar Strait are from [http://ocp.ldeo.columbia.edu/res/div/ocp/projects/MITF/cm\\_data/](http://ocp.ldeo.columbia.edu/res/div/ocp/projects/MITF/cm_data/), and the ASV data in the Halmahera Sea are from <http://itf.qdio.ac.cn/xzlxz/>. The altimeter data from CEMMS can be downloaded from <https://data.marine.copernicus.eu/products>. The daily NCDC blended wind products can be downloaded from <https://www.ncei.noaa.gov/products/blended-sea-winds>. Niño 3.4 index and DMI provided by Climate Prediction Center, Physical Sciences Laboratory, NOAA and JAMSTEC (Japan Agency for Marine-earth Science and Technology) are from <https://www.cpc.ncep.noaa.gov/data/indices/>, <https://psl.noaa.gov/data/correlation/pdo.data>, and <https://www.jamstec.go.jp/virtualearth/general/en/index.html>, respectively.

## Acknowledgments

This study was supported by the Strategic Priority Research Program of Chinese Academy of Sciences (Project No. XDB42000000) and the National Natural Science Foundation of China (NSFC) 42106018. We thank CMEMS and NDC, NOAA for providing the altimeter and blended wind products, respectively. We also thank Climate Prediction Center, Physical Sciences Laboratory, NOAA and JAMSTEC (Japan Agency for Marine-earth Science and Technology) for providing the Niño 3.4 index, PDO index, and DMI. The mooring data in the Makassar Strait and the ASV data in the Halmahera Sea are shared by Lamont-Doherty Earth Observatory and Institute of Oceanology, Chinese Academy of Sciences, respectively. We also thank Artur P. Palacz for sharing the code of EEMD analysis for this study.

## References

- Alexander, M. A., Bladé, I., Newman, M., Lanzante, J. R., Lau, N. C., & Scott, J. D. (2002). The atmospheric bridge: The influence of ENSO teleconnections on air-sea interaction over the global oceans. *Journal of Climate*, 15(16), 2205–2231. [https://doi.org/10.1175/1520-0442\(2002\)015<2205:tabtio>2.0.co;2](https://doi.org/10.1175/1520-0442(2002)015<2205:tabtio>2.0.co;2)
- Boulanger, J., & Menkes, C. (1995). Propagation and reflection of long equatorial waves in the Pacific Ocean during the 1992–1993 El Niño. *Journal of Geophysical Research*, 100(C12), 25041–25059. <https://doi.org/10.1029/95JC02956>
- Clarke, A. J. (1991). On the reflection and transmission of low-frequency energy at the irregular western Pacific Ocean boundary. *Journal of Geophysical Research*, 96(S1), 3289–3305. <https://doi.org/10.1029/90JC00985>
- Clarke, A. J., & Liu, X. (1994). Interannual sea level in the northern and eastern Indian Ocean. *Journal of Physical Oceanography*, 24(6), 1224–1235. [https://doi.org/10.1175/1520-0485\(1994\)024<1224:isltin>2.0.co;2](https://doi.org/10.1175/1520-0485(1994)024<1224:isltin>2.0.co;2)
- Drushka, K., Sprintall, J., Gille, S. T., & Brodjonegoro, I. (2010). Vertical structure of Kelvin waves in the Indonesian Throughflow exit passages. *Journal of Physical Oceanography*, 40(9), 1965–1987. <https://doi.org/10.1175/2010JPO4380.1>
- du Penhoat, Y., & Cane, M. A. (1991). Effect of low-latitude western boundary gaps on the reflection of equatorial motions. *Journal of Geophysical Research*, 96(S1), 3307–3322. <https://doi.org/10.1029/90JC01798>
- England, M. H., & Huang, F. (2005). On the interannual variability of the Indonesian Throughflow and its linkage with ENSO. *Journal of Climate*, 18(9), 1435–1444. <https://doi.org/10.1175/JCLI3322.1>
- Feng, M., McPhaden, M. J., Xie, S.-P., & Hafner, J. (2013). La Niña forces unprecedented Leeuwin Current warming in 2011. *Scientific Reports*, 3(1), 1277. <https://doi.org/10.1038/srep01277>
- Fine, R., Lukas, R., Bingham, F. M., Warner, M. J., & Gammon, R. H. (1994). The western equatorial Pacific: A water mass crossroads. *Journal of Geophysical Research*, 99(C12), 25063–25080. <https://doi.org/10.1029/94JC02277>
- Godfrey, J. (1996). The effect of the Indonesian Throughflow on ocean circulation and heat exchange with the atmosphere: A review. *Journal of Geophysical Research*, 101(C5), 12217–12237. <https://doi.org/10.1029/95JC03860>
- Gordon, A. L. (2005). Oceanography of the Indonesian seas and their throughflow. *Oceanography*, 18(4), 14–27. <https://doi.org/10.5670/oceanog.2005.01>
- Gordon, A. L., Huber, B. A., Metzger, E. J., Susanto, R. D., Hurlburt, H. E., & Adi, T. R. (2012). South China Sea throughflow impact on the Indonesian Throughflow. *Geophysical Research Letters*, 39(11), 117–128. <https://doi.org/10.1029/2012GL052021>
- Gordon, A. L., Napitu, A., Huber, B. A., Gruenburg, L. K., Pujana, K., Agustiad, T., et al. (2019). Makassar Strait throughflow seasonal and interannual variability: An overview. *Journal of Geophysical Research: Oceans*, 124(6), 3724–3736. <https://doi.org/10.1029/2018JC014502>
- Gordon, A. L., Sprintall, J., Van Aken, H. M., Susanto, D., Wijffels, S., Molcard, R., et al. (2010). The Indonesian Throughflow during 2004–2006 as observed by the INSTANT program. *Dynamics of Atmospheres and Oceans*, 50(2), 115–128. <https://doi.org/10.1016/j.dynatmoce.2009.12.002>
- Gordon, A. L., Susanto, R. D., & Ffield, A. (1999). Throughflow within Makassar Strait. *Geophysical Research Letters*, 26(21), 3325–3328. <https://doi.org/10.1029/1999GL002340>
- Gordon, A. L., Susanto, R. D., Ffield, A., & Pillsbury, D. (1998). Makassar Strait transport: Preliminary Arlindo results from MAK1 and MAK2. *International WOCE Newsletter*, 33, 30–32.
- Gordon, A. L., Susanto, R. D., Ffield, A., Huber, B. A., Pranowo, W., & Wirasantosa, S. (2008). Makassar Strait throughflow, 2004 to 2006. *Geophysical Research Letters*, 35(24), 851–854. <https://doi.org/10.1029/2008GL036372>
- Hu, D., Wu, L., Cai, W., Gupta, A. S., Ganachaud, A., Qiu, B., et al. (2015). Pacific western boundary currents and their roles in climate. *Nature*, 522(7556), 299–308. <https://doi.org/10.1038/nature14504>
- Hu, X., Sprintall, J., Yuan, D., Tranchant, B., Gaspar, P., Koch-Larrouy, A., et al. (2019). Interannual variability of the Sulawesi Sea circulation forced by Indo-Pacific planetary waves. *Journal of Geophysical Research: Oceans*, 124(3), 1616–1633. <https://doi.org/10.1029/2018JC014356>
- Izumo, T., Vialard, J., Lengaigne, M., de Boyer Montegut, C., Behera, S. K., Luo, J. J., et al. (2010). Influence of the state of the Indian Ocean Dipole on the following year's El Niño. *Nature Geoscience*, 3, 168–172. <https://doi.org/10.1038/ngeo760>
- Kashino, Y., Atmadipoera, A., Kuroda, Y., & Lukijanto (2013). Observed features of the Halmahera and Mindanao Eddies. *Journal of Geophysical Research: Oceans*, 118(12), 6543–6560. <https://doi.org/10.1002/2013JC009207>
- Kashino, Y., España, N., Syamsudin, F., Richards, K. J., Jensen, T., Dutrieux, P., & Ishida, A. (2009). Observations of the North Equatorial current, Mindanao current, and Kuroshio current system during the 2006/07 El Niño and 2007/08 La Niña. *Journal of Oceanography*, 65(3), 325–333. <https://doi.org/10.1007/s10872-009-0030-z>
- Kataoka, T., Tozuka, T., Behera, S., & Yamagata, T. (2014). On the Ningaloo Niño/Niña. *Climate Dynamics*, 43(5–6), 1463–1482. <https://doi.org/10.1007/s00382-013-1961-z>
- Klein, S. A., Soden, B. J., & Lau, N.-C. (1999). Remote sea surface temperature variations during ENSO: Evidence for a tropical atmospheric bridge. *Journal of Climate*, 12(4), 917–932. [https://doi.org/10.1175/1520-0442\(1999\)012<0917:rsstvd>2.0.co;2](https://doi.org/10.1175/1520-0442(1999)012<0917:rsstvd>2.0.co;2)
- Kusunoki, H., Kido, S., & Tozuka, T. (2020). Contribution of oceanic wave propagation from the tropical Pacific to asymmetry of the Ningaloo Niño/Niña. *Climate Dynamics*, 54(11–12), 4865–4875. <https://doi.org/10.1007/s00382-020-05268-5>
- Lau, N.-C., & Nath, M. J. (2003). Atmosphere-ocean variations in the Indo-Pacific sector during ENSO episodes. *Journal of Climate*, 16(1), 3–20. [https://doi.org/10.1175/1520-0442\(2003\)0162.0.CO;2](https://doi.org/10.1175/1520-0442(2003)0162.0.CO;2)
- Li, M., Gordon, A. L., Gruenburg, L. K., Wei, J., & Yang, S. (2020). Interannual to decadal response of the Indonesian Throughflow vertical profile to Indo-Pacific forcing. *Geophysical Research Letters*, 47(11), e2020GL087679. <https://doi.org/10.1029/2020GL087679>
- Li, M., Xue, H., Wei, J., Liang, L., Gordon, A. L., & Yang, S. (2021). The role of the Mindoro-Sibutu pathway on the South China Sea multi-layer circulation. *Journal of Physical Oceanography*, 51, 2767–2782. <https://doi.org/10.1175/JPO-D-20-0165.1>
- Li, M., Yuan, D., Gordon, A. L., Gruenburg, L. K., Li, X., Li, R., et al. (2021). A strong sub-thermocline intrusion of the North Equatorial Subsurface Current into the Makassar Strait in 2016–2017. *Geophysical Research Letters*, 48(8), e2021GL092505. <https://doi.org/10.1029/2021GL092505>
- Li, X., Yuan, D., Li, Y., Wang, Z., Wang, J., Hu, X., et al. (2021). Moored observations of currents and water mass properties between Talaud and Halmahera Islands at the entrance of the Indonesian Seas. *Journal of Physical Oceanography*, 51, 3557–3572. <https://doi.org/10.1175/JPO-D-21-0048.1>
- Li, X., Yuan, D., Wang, Z., Li, Y., Corvianawatie, C., Surinati, D., et al. (2020). Moored observations of transport and variability of Halmahera Sea currents. *Journal of Physical Oceanography*, 50(2), 471–488. <https://doi.org/10.1175/JPO-D-19-0109.1>
- Liang, L., & Xue, H. (2020). The Reversal Indian Ocean Waters. *Geophysical Research Letters*, 47(14), e2020GL088269. <https://doi.org/10.1029/2020GL088269>
- Liang, L., Xue, H., & Shu, Y. (2019). The Indonesian Throughflow and the circulation in the Banda Sea: A modeling study. *Journal of Geophysical Research: Oceans*, 124(5), 3089–3106. <https://doi.org/10.1029/2018JC014926>

- Lindstrom, E., Lukas, R., Fine, R., Firing, E., Godfrey, S., Meyers, G., & Tsuchiya, M. (1987). The western equatorial Pacific Ocean circulation study. *Nature*, 330(6148), 533–537. <https://doi.org/10.1038/330533a0>
- Liu, Q. Y., Feng, M., Wang, D., & Wijffels, S. (2015). Interannual variability of the Indonesian Throughflow transport: A revisit based on 30 year expendable bathythermograph data. *Journal of Geophysical Research: Oceans*, 120(12), 8270–8282. <https://doi.org/10.1002/2015JC011351>
- Ma, Q., Wang, J., Wang, F., Zhang, D., Zhang, Z., & Lyu, Y. (2020). Interannual variability of lower equatorial intermediate current response to ENSO in the Western Pacific. *Geophysical Research Letters*, 47(16), e2020GL089311. <https://doi.org/10.1029/2020GL089311>
- McClean, J. L., Ivanova, D. P., & Sprintall, J. (2005). Remote origins of interannual variability in the Indonesian Throughflow region from data and a global Parallel Ocean Program simulation. *Journal of Geophysical Research*, 110(C10), C10013. <https://doi.org/10.1029/2004JC002477>
- McCreary, J. P. (1981). A linear stratified ocean model of the equatorial undercurrent. *Philosophical Transactions of the Royal Society A: Mathematical, Physical & Engineering Sciences*, 298, 603–635. <https://doi.org/10.1098/rsta.1981.0002>
- Meyers, G. (1996). Variation of Indonesian Throughflow and the El Niño–Southern Oscillation. *Journal of Geophysical Research*, 101(C5), 12255–12263. <https://doi.org/10.1029/95JC03729>
- Palacz, A. P., Xue, H., Armbricht, C., Zhang, C., & Chai, F. (2011). Seasonal and inter-annual changes in the surface chlorophyll of the South China Sea. *Journal of Geophysical Research*, 106(C9), C09015. <https://doi.org/10.1029/2011JC007064>
- Pujiana, K., Gordon, A. L., & Sprintall, J. (2013). Intraseasonal Kelvin wave in Makassar Strait. *Journal of Geophysical Research: Oceans*, 118(4), 2023–2034. <https://doi.org/10.1002/jgrc.20069>
- Pujiana, K., McPhaden, M. J., Gordon, A. L., & Napitu, A. M. (2019). Unprecedented response of Indonesian Throughflow to anomalous Indo-Pacific climatic forcing in 2016. *Journal of Geophysical Research: Oceans*, 124(6), 3737–3754. <https://doi.org/10.1029/2018JC014574>
- Qu, T., & Lindstrom, E. (2004). Northward intrusion of Antarctic intermediate water in the western Pacific. *Journal of Physical Oceanography*, 34(9), 2104–2118. [https://doi.org/10.1175/1520-0485\(2004\)034<2104:mioaiw>2.0.co;2](https://doi.org/10.1175/1520-0485(2004)034<2104:mioaiw>2.0.co;2)
- Saji, N., Goswami, B. N., Vinayachandran, P., & Yamagata, T. (1999). A dipole mode in the tropical Indian Ocean. *Nature*, 401(6751), 360–363. <https://doi.org/10.1038/43854>
- Schneider, N. (1998). The Indonesian Throughflow and the global climate system. *Journal of Climate*, 11(4), 676–689. [https://doi.org/10.1175/1520-0442\(1998\)011<0676:titatg>2.0.co;2](https://doi.org/10.1175/1520-0442(1998)011<0676:titatg>2.0.co;2)
- Spall, M. A., & Pedlosky, J. (2005). Reflection and transmission of equatorial Rossby waves. *Journal of Physical Oceanography*, 35(3), 363–373. <https://doi.org/10.1175/JPO-2691.1>
- Sprintall, J., Chong, J., Syamsudin, F., Morawitz, W., Hautala, S., Bray, N., & Wijffels, S. (1999). Dynamics of the South Java Current in the Indo-Australian Basin. *Geophysical Research Letters*, 26(16), 2493–2496. <https://doi.org/10.1029/1999GL002320>
- Sprintall, J., Gordon, A. L., Koch-Larrouy, A., Lee, T., Potemra, J. T., Pujiana, K., & Wijffels, S. E. (2014). The Indonesian seas and their role in the coupled ocean–climate system. *Nature Geoscience*, 7, 487–492. <https://doi.org/10.1038/ngeo2188>
- Sprintall, J., Gordon, A. L., Wijffels, S., Feng, M., Hu, S., Koch-Larrouy, A., et al. (2019). Detecting change in the Indonesian seas. *Frontiers in Marine Science*, 6, 257. <https://doi.org/10.3389/fmars.2019.00257>
- Sprintall, J., Wijffels, S., Gordon, A. L., Ffield, A., Molcard, R., Susanto, R. D., et al. (2004). INSTANT: A new international array to measure the Indonesian Throughflow. *EOS, Transactions American Geophysical Union*, 85(39), 369–376. <https://doi.org/10.1029/2004EO390002>
- Sprintall, J., Wijffels, S. E., Molcard, R., & Jaya, I. (2009). Direct estimates of the Indonesian Throughflow entering the Indian Ocean: 2004–2006. *Journal of Geophysical Research*, 114(C7), C07001. <https://doi.org/10.1029/2008JC005257>
- Susanto, R. D., Ffield, A., Gordon, A. L., & Adi, T. R. (2012). Variability of Indonesian Throughflow within Makassar Strait, 2004–2009. *Journal of Geophysical Research*, 117(C9). <https://doi.org/10.1029/2012JC008096>
- Susanto, R. D., & Gordon, A. L. (2005). Velocity and transport of the Makassar Strait throughflow. *Journal of Geophysical Research*, 110(C1), C01005. <https://doi.org/10.1029/2004JC002425>
- Susanto, R. D., Gordon, A. L., Sprintall, J., & Herunadi, B. (2000). Intraseasonal variability and tides in Makassar Strait. *Geophysical Research Letters*, 27(10), 1499–1502. <https://doi.org/10.1029/2000GL011414>
- Trenberth, K. E. (1997). The definition of El Niño. *Bulletin of the American Meteorological Society*, 78(12), 2771–2778. [https://doi.org/10.1175/1520-0477\(1997\)078<2771:tdoeno>2.0.co;2](https://doi.org/10.1175/1520-0477(1997)078<2771:tdoeno>2.0.co;2)
- Wang, C. (2019). Three-ocean interactions and climate variability: A review and perspective. *Climate Dynamics*, 53(7–8), 5119–5136. <https://doi.org/10.1007/s00382-019-04930-x>
- Wang, J., Yuan, D., Li, X., Li, Y., Wang, Z., Hu, X., et al. (2020). Moored observations of the Savu Strait currents in the Indonesian seas. *Journal of Geophysical Research: Oceans*, 125(7), e2020JC016082. <https://doi.org/10.1029/2020JC016082>
- Wang, Z., & Yuan, D. (2012). Nonlinear dynamics of two western boundary currents colliding at a gap. *Journal of Physical Oceanography*, 42(11), 2030–2040. <https://doi.org/10.1175/JPO-D-12-05.1>
- Wang, Z., & Yuan, D. (2014). Multiple equilibria and hysteresis of two unequal-transport western boundary currents colliding at a gap. *Journal of Physical Oceanography*, 44(7), 1873–1885. <https://doi.org/10.1175/JPO-D-13-0234.1>
- Wijffels, S., & Meyers, G. (2004). An intersection of oceanic waveguides: Variability in the Indonesian Throughflow region. *Journal of Physical Oceanography*, 34(5), 1232–1253. [https://doi.org/10.1175/1520-0485\(2004\)034<1232:aioovv>2.0.co;2](https://doi.org/10.1175/1520-0485(2004)034<1232:aioovv>2.0.co;2)
- Wu, Z., & Huang, N. E. (2009). Ensemble empirical mode decomposition: A noise assisted data analysis method. *Advances in Adaptive Data Analysis*, 1(1), 1–41. <https://doi.org/10.1142/S1793536909000047>
- Yuan, D., & Han, W. (2006). Roles of Equatorial waves and western boundary reflection in the seasonal circulation of the equatorial Indian Ocean. *Journal of Physical Oceanography*, 36(5), 930–944. <https://doi.org/10.1175/JPO2905.1>
- Yuan, D., Hu, X., Xu, P., Zhao, X., Masumoto, Y., & Han, W. (2018). The IOD–ENSO precursory teleconnection over the tropical Indo-Pacific Ocean: Dynamics and long-term trends under global warming. *Journal of Oceanology and Limnology*, 36(1), 4–19. <https://doi.org/10.1007/s00343-018-6252-4>
- Yuan, D., Rienecker, M. M., & Schopf, P. S. (2004). Long wave dynamics of the interannual variability in a numerical hindcast of the equatorial Pacific Ocean circulation during the 1990s. *Journal of Geophysical Research*, 109(C5), C05019. <https://doi.org/10.1029/2003JC001936>
- Yuan, D., Song, X., Yang, Y., & Dewar, W. K. (2019). Dynamics of mesoscale eddies interacting with a western boundary current flowing by a gap. *Journal of Geophysical Research: Oceans*, 124(6), 4117–4132. <https://doi.org/10.1029/2019JC014949>
- Yuan, D., Wang, J., Xu, T., Xu, P., Hui, Z., Zhao, X., et al. (2011). Forcing of the Indian Ocean Dipole on the interannual variations of the tropical Pacific Ocean: Roles of the Indonesian Throughflow. *Journal of Climate*, 24(14), 3593–3608. <https://doi.org/10.1175/2011JCLI3649.1>
- Yuan, D., & Wang, Z. (2011). Hysteresis and dynamics of a western boundary current flowing by a gap forced by impingement of mesoscale eddies. *Journal of Physical Oceanography*, 41(5), 878–888. <https://doi.org/10.1175/2010JPO4489.1>
- Yuan, D., Yin, X., Li, X., Corvianawatie, C., Wang, Z., Li, Y., et al. (2022). A Maluku Sea intermediate western boundary current connecting Pacific Ocean circulation to the Indonesian Throughflow. *Nature Communications*, 13(1), 2093. <https://doi.org/10.1038/s41467-022-29617-6>



- Yuan, D., Zhou, H., & Zhao, X. (2013). Interannual climate variability over the tropical Pacific Ocean induced by the Indian Ocean dipole through the Indonesian Throughflow. *Journal of Climate*, 26(9), 2845–2861. <https://doi.org/10.1175/JCLI-D-12-00117.1>
- Zhang, L., & Han, W. (2018). Impact of Ningaloo Niño on tropical Pacific and an interbasin coupling mechanism. *Geophysical Research Letters*, 45(20), 11300–11309. <https://doi.org/10.1029/2018GL078579>

### References From the Supporting Information

- Lee, T., Fournier, S., Gordon, A. L., & Sprintall, J. (2019). Maritime Continent water cycle regulates low-latitude chokepoint of global ocean circulation. *Nature Communication*, 10, 2103. <https://doi.org/10.1038/s41467-019-10109-z>